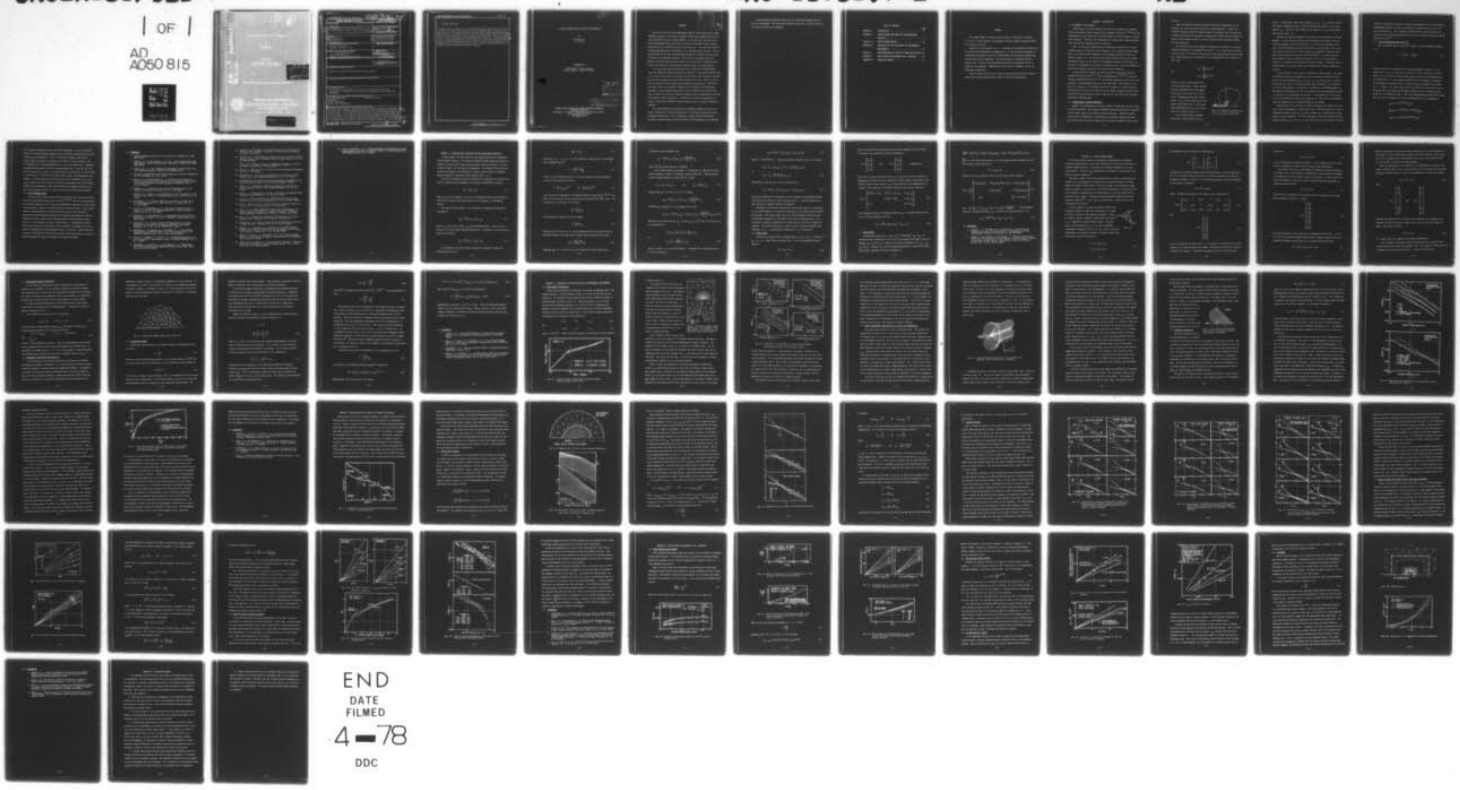
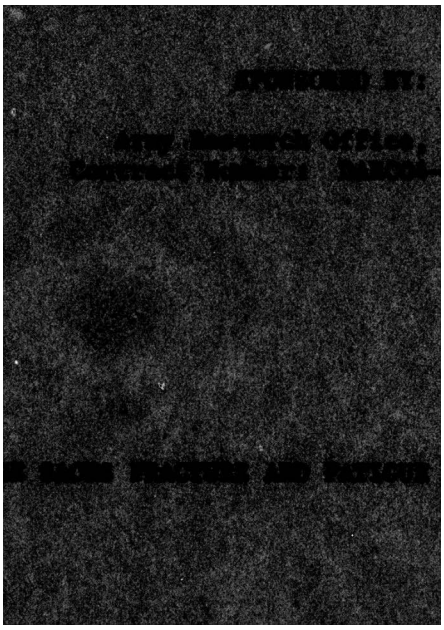
AD-A050 815 SYRACUSE UNIV N Y DEPT OF CHEMICAL ENGINEERING AND --ETC F/G 20/11
A FINITE ELEMENT STUDY ON CRACK TIP DEFORMATION.(U)
AUG 76 W HU, H W LIU DAHC04-74-G-0165
UNCLASSIFIED ARO-11961.7-E NL

1 OF 1
AD A050 815



END
DATE FILMED
4-78
DDC



Unclassified
SECURITY CLASSIFICATION OF THIS PAGE (When Data Entered)

(18) ARO (19) 11961.7-E

REPORT DOCUMENTATION PAGE

READ INSTRUCTIONS BEFORE COMPLETING FORM

1. REPORT NUMBER: 11961.7-E	2. GOVT ACCESSION NO.
3. RECIPIENT'S CATALOG NUMBER	
4. TITLE (and Subtitle): (6) A Finite Element Study on Crack Tip Deformation.	5. TYPE OF REPORT & PERIOD COVERED: (9) Technical Report.
	6. PERFORMING ORG. REPORT NUMBER
7. AUTHOR(s): (10) Wan-liang Hu, H. W. Liu	8. CONTRACT OR GRANT NUMBER(s): (15) DAHC04-74-G-0165
9. PERFORMING ORGANIZATION NAME AND ADDRESS: Syracuse University, Syracuse, New York 13210	10. PROGRAM ELEMENT, PROJECT, TASK AREA & WORK UNIT NUMBERS
11. CONTROLLING OFFICE NAME AND ADDRESS: U. S. Army Research Office, Post Office Box 12211, Research Triangle Park, NC 27709	12. REPORT DATE: (11) Aug 76 13. NUMBER OF PAGES: 63 (12) 71p.
14. MONITORING AGENCY NAME & ADDRESS (If different from Controlling Office)	15. SECURITY CLASS. (of this report): Unclassified 15a. DECLASSIFICATION/DOWNGRADING SCHEDULE

16. DISTRIBUTION STATEMENT (of this Report)

Approved for public release; distribution unlimited.

17. DISTRIBUTION STATEMENT (of the abstract entered in Block 20, if different from Report)

18. SUPPLEMENTARY NOTES

The findings in this report are not to be construed as an official Department of the Army position, unless so designated by other authorized documents.

19. KEY WORDS (Continue on reverse side if necessary and identify by block number)

Cracking(fracturing)
Deformation
Plastic deformation
Stress strain distribution
Fracture properties

20. ABSTRACT (Continue on reverse side if necessary and identify by block number)

The moire crack tip strain measurements made on double-edge-notched specimens loaded into the region of general yielding are compared with the results calculated by finite element method. It is found that the bulk of the strain measurements agree well with the results of the plane stress calculations except in the small area close to the crack tip. The crack tip region is stiffened against plastic deformation by the triaxial state of stress. The region affected by the crack tip stiffening extends to a distance from the crack tip equal to the specimen thickness. This crack tip

DD FORM 1 JAN 73 1473 EDITION OF 1 NOV 65 IS OBSOLETE

Unclassified 406 796
SECURITY CLASSIFICATION OF THIS PAGE (When Data Entered)

20. ABSTRACT CONTINUED

stiffened zone is embedded in the characteristic plane stress zone if the ratio of specimen thickness and the total net cross-sectional width is equal to or more than ten. The stress and strain distributions in the plastically deformed region under the condition of plane stress are investigated. The results indicate that the size of the plastic zone along the crack line can be used as a scaling factor for the stress and strain field around the crack tip. A link between linear elastic fracture mechanics and ductile fracture criterion for the case of general yielding could be established by the near tip stress or strain correlation. A closed form solution relating near tip stress or strain with equivalent stress intensity factor in general yielding is obtained.

(5)

A FINITE ELEMENT STUDY ON CRACK TIP DEFORMATION

by

Wan-liang Hu
H. W. Liu

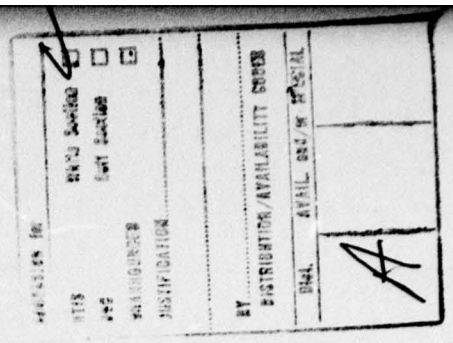
SPONSORED BY:

Army Research Office, Durham
Contract Number: DAHC04-74-G-0165

DDC
RECEIVED
MAR 7 1978
A

DISTRIBUTION STATEMENT A
Approved for public release;
Distribution Unlimited

GEORGE SACHS FRACTURE AND FATIGUE RESEARCH LABORATORY
SYRACUSE UNIVERSITY
Department of Chemical Engineering and Materials Science
Syracuse, New York 13210
MS-HWL-1607-876



ABSTRACT

The moire crack tip strain measurements made on double-edge-notched (DEN) specimens loaded into the region of general yielding are compared with the results calculated by finite element method. It is found that the bulk of the strain measurements agree well with the results of the plane stress calculations except in the small area close to the crack tip. The crack tip region is stiffened against plastic deformation by the triaxial state of stress. The region affected by the crack tip stiffening extends to a distance from the crack tip equal to the specimen thickness. This crack tip stiffened zone is embedded in the characteristic plane stress zone if the ratio of specimen thickness and the total net cross-sectional width is equal to or more than ten.

The stress and strain distributions in the plastically deformed region under the condition of plane stress are investigated. The results indicate that r_p, the size of the plastic zone along the crack line, can be used as a scaling factor for the stress and strain field around the crack tip. This is true in both of the small scale yielding case and general yielding case. The size of the plastic zone in the general yielding case is obtained by extrapolation. Therefore, a link between linear elastic fracture mechanics and ductile fracture criterion for the case of general yielding could be established by the near tip stress or strain correlation. A closed form solution relating near tip stess or strain with equivalent stress intensity factor in general yielding is obtained.

In a region beyond the initial point of general yielding, the near tip stress and strain are linearly proportional to the applied stress and overall elongation respectively. As a consequence, a simple relation between the equivalent stress intensity factor and the far field parameters is established

Crack opening displacements (COD) are also studied and compared with empirical measurements. The inter-relationships between COD, J-integral and near tip stress and strain are examined.

TABLE OF CONTENTS

		Page
CHAPTER I	INTRODUCTION	1
CHAPTER II	CONSTITUTIONAL RELATIONS FOR TWO-DIMENSIONAL PLASTICITY	9
CHAPTER III	FINITE ELEMENT METHOD.	15
CHAPTER IV	COMPARISON OF FEM CALCULATION AND EXPERIMENTAL MEASUREMENTS	24
CHAPTER V	CHARACTERIZATION OF CRACK TIP STRESS AND STRAINS	36
CHAPTER VI	CRACK OPENING DISPLACEMENTS AND J-INTEGRALS . .	53
CHAPTER VII	CONCLUDING REMARKS	62

PREFACE

The author wishes to extend a sincere thanks to his advisor, Professor H. W. Liu, for his continuous encouragement and many valuable guidances during the course of this work.

Thanks are also extended to Dr. J. L. Swedlow of Carnegie-Mellon University for his fruitful discussions and suggestions. It would be almost impossible to acknowledge individually each of the staff members of the Chemical Engineering and Materials Science Department. The author wishes to thank particularly, however, Mrs. H. Turner who painstakingly prepared the manuscript and Mr. R. Ziemer for the drawings. Thanks are also due to Mrs. H. DeMascio for her administrative assistance.

Special thanks are also due to both the American Iron and Steel Institute (AISI) and the Army Research Office (ARO) for the financial support.

CHAPTER I INTRODUCTION

1.1 STATEMENT OF THE PROBLEM

Linear elastic fracture mechanics has been very successful in analyzing fracture problems of high strength but low toughness materials.[1,2,3] One of the requirements for the validity of the linear elastic fracture mechanics is small scale yielding.[4] Therefore, the application of linear elastic fracture mechanics to ductile and tough materials is ruled out.

Prior to fracture, extensive plastic deformation takes place in a small testpiece made of a tough and ductile material. But a large structural member made of the same material containing a large enough crack may fracture in a "brittle" manner, i.e. the bulk of the structure remains elastic with plastic deformation limited to the region in the immediate vicinity of the crack tip. The lack of information on the plastic deformation near a crack tip prevents the correlation between the ductile and brittle fracture behavior.

During the past few years, the crack tip plastic deformation has been studied both theoretically[5,6,7,8,9] and experimentally.[10,11,12,13] Some preliminary comparisons were made.[12,14] The general qualitative trends of the calculations and measurements agree well with each other. The purpose of this study is to provide a link between the ductile fracture of a small testpiece and the brittle fracture of a large structural member through the study of the stress and strain distribution near a crack tip for both small scale yielding and general yielding cases.

1.2 LINEAR ELASTIC FRACTURE MECHANICS

Inglis[15] has determined the stresses around an elliptical hole in a plate of elastic materials. This pioneer mathematical work was employed by Griffith[16] in his classic paper on the theory of brittle fracture. Griffith's theory evolved from a consideration of minimizing the potential energy which takes into account both the elastic energy and the energy of formation of the crack

surface.

Almost all metallic materials manifest some plastic deformation in the region at the crack tip before catatrophic crack propagation. Irwin[17] and Orowan[18] reexamined Griffith's energy concept and proposed that his theory can be modified and applied to metals by considering the energy balance between the elastic strain energy release rate and the plastic strain work rate required for crack extension.

The character of the local stress distribution at the base of a crack was studied by Williams,[19] Westergaard[20] and Irwin.[21] It is found that the elastic stresses varies as the inverse square root of the radial distance from the crack tip. Their results can be summarized in the following Eqs., for a mode-I tensile crack

$$\sigma_{ij} = \frac{K_I}{\sqrt{2\pi r}} f_{ij}(\theta)$$

and 1-1

$$\varepsilon_{ij} = \frac{K_I}{\sqrt{2\pi r}} g_{ij}(\theta)$$

where K_I is the stress intensity factor under tensile mode. These relations are good approximations in the region very close to the crack tip of an isotropic, homogeneous and linear elastic solid. Let r_e be the linear size of the region within which Eqs. 1-1 are acceptable approximations, and r_e is a function of θ as shown in Fig. 1-1.

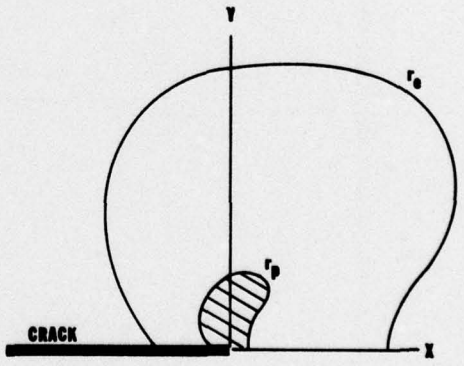


Fig. 1-1 Schematic representation of r_e and r_p near a crack tip.

In a cracked metallic specimen under load, a small plastic zone, r_p,

exists. In the case of small scale yielding, $r_p < r_e$. If r_p is small enough, the plastic deformation within r_p does not disturb the stresses in the outer region of r_e. Therefore, the stresses on the boundary of r_e are essentially those given by Eqs. 1-1.

Consider two cracked specimens of the same thickness and made of the same material. If the condition of small scale yielding is satisfied by both of these two specimens, and if the values of K_I of these two specimens are the same, then the stresses and strains even within r_p are the same. This can be seen easily if one considers the two identical r_e regions of these two specimens as free bodies with identical boundary stresses. At a given K_I-value, with identical crack tip stresses and strains, if one of the specimens is broken, it is expected that the other will also be broken. Therefore, one can conclude that in the case of small scale yielding, the fracture toughness is constant.

This conclusion is valid only for specimens of same thickness. The specimen thickness affects the constraint to plate thickness contraction and the stress and strain components σ_{zz}, σ_{xz}, σ_{yz}, ε_{zz}, ε_{xz} and ε_{yz} near a crack tip. At the same K_I- value, in the case of small scale yielding, if the specimens are of the same thickness, in spite of the difference in specimen geometry in the other two dimensions, the crack tip stress, strain and displacement fields of every one of the specimens are the same. If the specimen is thick enough so that the condition of plane strain prevails at a crack tip, the requirement that the specimens be of the same thickness can be relaxed.

There exists a set of values of crack tip stresses and strains, even within r_p, which corresponds to a given value of K_I. The mere existence of the correspondence between K_I and σ_{ij}, ε_{ij} and u_i enables us to establish the linear elastic fracture mechanics. It is not necessary to know the detailed relations between K_I and σ_{ij}, ε_{ij}, and u_i. On the other hand, if the relations are known

either by theoretical calculation or empirical measurements, both crack opening displacement, (COD), or near tip strain, (NTS), at a single point P(r, θ) can be used to determine K_I. This concept of characterizing crack tip stresses and strains by COD and NTS was generalized to the case of general yielding by Wells[22] and Ke and Liu.[23,24]

1.3 PLASTIC DEFORMATION NEAR CRACK TIP

For a non-linear elastic body Rice[25] defined a path independent integral, J by

$$J \equiv \int_{\Gamma} [Wdy - \bar{T} \frac{\partial \bar{u}}{\partial x} ds] \qquad 1\text{-}2$$

where the curve Γ is tranversed in the counterclockwise direction, s is arc length and $\bar{T} \equiv \sigma_{ij} n_j$ is the traction vector on Γ with an outward unit normal vector n_j, and W and $\bar{u}$ are strain energy density function and displacement vector respectively. It is also demonstrated[26] that the J-integral is equivalent to the change in potential energy, U, when the notch is extended by an amount da, J = - dU/da. For a sharp crack, since the path may be chosen very close to the crack tip, the integral may be made to depend only on the crack tip singularity in the deformation field. With this understanding Hutchinson[27] has shown that the crack tip stresses, strains and displacements can be expressed as

$$\sigma_{ij}(r,\theta) = K r^{-N/(1+N)} \tilde{\sigma}_{ij}(\theta)$$

$$\varepsilon^p_{ij}(r,\theta) = A^{-1/N} K^{1/N} r^{-1/(1+N)} \tilde{\varepsilon}^p_{ij}(\theta) \qquad 1\text{-}3$$

$$u_i(r,\theta) = A^{-1/N} K^{1/N} r^{N/(1+N)} \tilde{u}_i(\theta)$$

for a material obeying the power law strain hardening, i.e. $\sigma/\sigma_Y = A(\varepsilon^p/\varepsilon_Y)^N$. Where N is strain hardening exponent, and K is defined by Hutchinson as the amplitude of the singularity. K and J are directly related to each other. $\bar{\sigma}_{ij}(\theta)$, $\bar{\varepsilon}^p_{ij}(\theta)$ and $\bar{u}_i(\theta)$ are functions of θ only for a given material. Eqs. 1-3 indicate that a single parameter K or J, as in the elastic case, completely prescribes the stresses, strains and displacements near a crack tip, and also that if anyone of σ_{ij}, ε^p_{ij}, u_i at a point $P(r,\theta)$, is known, Eqs. 1-3 can be used to calculate K or J and all of the other stress, strain, and displacement components. In other words, the value of any one of the components of σ_{ij}, ε^p_{ij}, u_i at a single point can be used to completely characterize crack tip stresses, strains and displacements. This result affords the strongest analytical support for the general concept of crack tip stress and strain characterization.

1.4 FINITE ELEMENT METHOD

In recent years, finite element methods are widely used to study the stress and strain distribution around notch or crack.[28,29,30] Most of the calculations are confined primarily to the limiting two-dimensional conditions of plane stress or plane strain. Owing to the vastly increased computing effort, a very limited number of three-dimensional elasto-plastic calculations have been made.[31] Lacking such three-dimensional analyses, the present understanding of fracture mechanics is based largely on the limiting states of plane stress and plane strain. In the following sections, a model based on kinematically coupled plane stress and plane strain layers for the elements is employed in the calculation to simulate the three-dimensional effect of crack tip. Plane stress calculation in both general yielding case and small scale yielding case are made to study the stress and strain correlation in the near tip region.

1.5 REFERENCES

1. Fracture Toughness Testing and Its Applications, ASTM-STP 381, ASTM-NASA (1965).

2. Brown, W. F., Jr. and Srawley, J. E., eds., "Plane Strain Crack Toughness Testing of High Strength Metallic Materials," ASTM-STP 410, ASTM-NASA (1966).

3. Brown, W. F., Jr., eds., "Review of Developments in Plane Strain Fracture Toughness Testing," ASTM-STP 463, ASTM-NASA (1970).

4. Liu, H. W., "Discussion to 'A Critical Appraisal of Fracture Mechanics," STP 381, ASTM-NASA, pp. 23-26 (1965).

5. Hult, J. A. H. and McClintock, F. A., "Elastic-Plastic Stress and Strain Distributions Around Sharp Notches Under Repeated Shear," Ninth International Congress for Applied Mechanics, (Brussels), vol. 8, pp. 51-58 (1956).

6. Dugdale, D. S., "Yielding of Steel Sheets Containing Slits," Jour. Mechanics and Physics of Solids, vol. 8, p. 100 (1960).

7. Bilby, B. A., Cottrell, A. H. and Swinden, K. H., "The Spread of Plastic Yield from a Notch," Proceedings Royal Society, Series A, vol. 272, (1963).

8. Hutchinson, J. W., "Singular Behavior at the End of a Tensile Crack in a Hardening Material," J. Mech. and Phys. of Solids, vol. 16, p. 13-31 (1968).

9. Rice, J. R. and Rosengren, A. F., "Plane Strain Deformation Near a Crack Tip in a Power Law Hardening Material," J. Mech. and Phys. of Solids, vol. 16, p. 1-12 (1968).

10. Underwood, J. H. and Kendall, D. P., "Measurement of the Strain Distribution in the Region of a Crack," presented to ASTM Committee E-24, March (1967).

11. Gerberich, W. W., "Plastic Strains and Energy Density in Cracked Plates Part I Experimental Technique and Results," Experimental Mechanics, vol. 4, No. 11, pp. 335-344, Nov. (1964).

12. Kobayashi, A. S., Engstrom, E. L. and Simon, B. R., "Crack Opening Displacements and Normal Strains in Centrally Notched Plates," Experimental Mechanics, vol. 9, No. 4, pp. 163-170 (1969).

13. Liu, H. W., Gavigan, W. J. and Ke, J. S., "An Engineering Analysis of Ductile Fracture," International Journal of Fracture Mechanics, vol. 6, No. 1 (1970).

14. Underwood, J. H., Swedlow, J. L. and Kendall, D. P., "Experimental and Analytical Strains in an Edge-Cracked Sheet," Eng. Fract. Mech., vol. 2, pp. 183-196 (1971).

15. Inglis, C. E., "Stresses in a Cracked Plate Due to the Presence of Cracks and Sharp Corners," Transaction of Naval Architects (London) vol. 60, p. 213 (1913).

16. Griffith, A. A., "The Phenomena of Rapture and Flow in Solids," Philosophical Transactions of the Royal Society (London) Series A, vol. 221, pp. 163-198 (1921).

17. Irwin, G. R., "Fracture Dynamics," Fracturing of Metals, Am. Society for Metals (Cleveland) pp. 147-166 (1948).

18. Orowan, E., "Energy Criteria of Fracture," Welding Research Supplement, vol. 20, p. 1575 (1955).

19. Williams, M. L., "On the Stress Distribution at the Base of a Stationary Crack," Jour. Applied Mechanics, vol. 24, No. 1 (1957).

20. Westergaard, H. M., "Bearing Pressures and Cracks," Transactions, Am. Society Mechanical Engrs., Jour. of Applied Mechanics (1939).

21. Irwin, G. R., "Analysis of Stresses and Strains Near the End of a Crack Traversing a Plate," Jour. Applied Mechanics, vol. 24, No. 3 (1957).

22. Wells, A. A., "Application of Fracture Mechanics at and Beyond General Yielding," British Welding J., p. 563, Nov. (1963).

23. Liu, H. W., "Fracture Criteria of Cracked Metallic Plate," International Journal of Fracture Mechanics, Vol. 2, pp. 393-399 (1966).

24. Ke, J. S. and Liu, H. W., "Near Tip Strain as a Ductile Fracture Criterion," Int. J. of Fracture, Vol. 7, p. 487 (1971).

25. Rice, J. R., "A Path Independent Integral and the Approximate Analysis of Strain Concentration by Notches and Cracks," Journal of Applied Mechanics, Transaction of ASME, pp. 379-386, June (1968).

26. Rice, J. R., "Mathematical Analysis in the Mechanics of Fracture," Liebowitz eds., Fracture, Vol. 2, Chapter 3, pp. 191-311.

27. Hutchinson, J. W., "Plastic Stress and Strain Fields at a Crack Tip," J. Mech. and Phys. of Solids, Vol. 16, pp. 337-347 (1968).

28. Swedlow, J. L., Williams, M. L. and Yang, W. E., "Elasto-Plastic Stresses and Strains in Cracked Plates," Proceedings of First Inter. Conf. on Fract., Sendai, Vol. 1, pp. 259-282 (1965).

29. Chan, S. K., Tuba, I. S. and Wilson, W. K., "On the Finite Element Method in Linear Fracture Mechanics," Engineering Fracture Mechanics, Vol. 2, pp. 1-17 (1970).

30. Marcal, P. V. and King, I. P., "Elastic-plastic Analysis of Two-Dimensional Stress Systems by the Finite Element Method," Int. J. Mech. Sci., Vol. 9, pp. 143-155 (1967).

31. Levy, N. and Marcal, P. V., "Three Dimensional Elastic-Plastic Stressed Strain Analysis for Fracture Mechanics, Phase II: Improved Modelling," HSST Technical Report No. 17 (1971).

CHAPTER II CONSTITUTIONAL RELATIONS FOR TWO-DIMENSIONAL PLASTICITY

In this chapter, we shall derive the governing equations for incremental elastic-plastic behavior. The explicit relations between stress and strain increments for both plane stress and plane strain cases are obtained. The continuum is taken to be isotropic and homogeneous. The thermal effects and body forces are excluded in the derivation. General tensor notation is employed. Repeated indices in subscripts imply summation over 1, 2, 3.

The total incremental strains are assumed to be separable into elastic and plastic components whose dependence upon stress is independently defined.

$$\dot{\varepsilon}_{ij} = \dot{\varepsilon}^{e}_{ij} + \dot{\varepsilon}^{p}_{ij} \quad , \tag{2-1}$$

where $\dot{\varepsilon}_{ij}$ are the components of the total incremental strains, $\dot{\varepsilon}^{e}_{ij}$ and $\dot{\varepsilon}^{p}_{ij}$ respectively the elastic and plastic parts of the components of incremental strains.

The linear elastic behavior of a continuum in Lagrangian variables are described by

$$\varepsilon^{e}_{ij} = \frac{1+\nu}{E}\,\sigma_{ij} - \frac{\nu}{E}\,\sigma_{\alpha\alpha}\,\delta_{ij} \quad , \tag{2-2}$$

where σ_{ij} is the stress tensor, δ_{ij} is the Kronecker delta, ν and E are the Poisson's ratio and Young's modulus respectively. Writing Eq. 2-2 in the incremental form, we have

$$\dot{\varepsilon}^{e}_{ij} = \frac{1+\nu}{E}\,\dot{\sigma}_{ij} - \frac{\nu}{E}\,\dot{\sigma}_{\alpha\alpha}\,\delta_{ij} \quad . \tag{2-3}$$

The components of plastic strain increment are assumed to follow the Prandtl-Reuss flow role

$$\dot{\varepsilon}^p_{ij} = \dot{\lambda}\, S_{ij} \quad , \tag{2-4}$$

where $S_{ij} = \sigma_{ij} - \sigma_{\alpha\alpha}\,\delta_{ij}/3$ are the deviatoric stresses and $\dot{\lambda}$ is the compliance increment given by

$$\dot{\lambda} = \frac{3}{2}\frac{\dot{\bar{\varepsilon}}^p}{\bar{\sigma}} = \frac{3}{2}\frac{\dot{\bar{\sigma}}}{\bar{\sigma}H} \quad . \tag{2-5}$$

In Eq. 2-5, the effective stress, $\bar{\sigma}$, and the incremental effective plastic strain, $\dot{\bar{\varepsilon}}^p$, are defined as follows:

$$\bar{\sigma} \equiv \left(\frac{3}{2} S_{ij}\, S_{ij}\right)^{1/2} \quad , \qquad \dot{\bar{\varepsilon}}^p \equiv \left(\frac{2}{3}\dot{\varepsilon}^p_{ij}\,\dot{\varepsilon}^p_{ij}\right)^{1/2} \quad , \tag{2-6}$$

where $\dot{\varepsilon}^p_{ij}$ are the components of incremental plastic strains and $H = \dot{\bar{\sigma}}/\dot{\bar{\varepsilon}}^p$ is the slope of the effective stress versus effective plastic strain, $\int \dot{\bar{\varepsilon}}^p$, curve. Substituting Eq. 2-5 into Eq. 2-4, we have

$$\dot{\varepsilon}^p_{ij} = \frac{3}{2}\frac{\dot{\bar{\sigma}}}{\bar{\sigma}H} S_{ij} \quad . \tag{2-7}$$

The derivative of effective stress is simply

$$\dot{\bar{\sigma}} = \frac{3}{2}\frac{S_{ij}}{\bar{\sigma}}\dot{S}_{ij} \quad . \tag{2-8}$$

Substitute Eq. 2-8 into Eq. 2-7, the incremental plastic strains are then expressed in terms of the incremental stresses and the current stress state

$$\dot{\varepsilon}^p_{ij} = \frac{9}{4}\frac{S_{kl}\,\dot{S}_{kl}}{\bar{\sigma}^2\, H} S_{ij} \quad . \tag{2-9}$$

Combining Eqs. 2-1, 2-3 and 2-9, we now formulate the basic constitutive

relations in the incremental form

$$\dot{\varepsilon}_{ij} = \frac{1+\nu}{E}\dot{\sigma}_{ij} - \frac{\nu}{E}\dot{\sigma}_{kk}\,\delta_{ij} + \frac{9}{4}\frac{S_{kl}\,\dot{S}_{kl}}{\bar{\sigma}^2\,H}\,S_{ij} \quad , \qquad 2\text{-}10$$

which has been derived earlier by Swedlow[1].

In the finite element calculation, it is desirable to express the incremental stresses in terms of incremental strains explicitly. From the definitions of stress deviator and bulk modulus, we have

$$\dot{\sigma}_{ij} \equiv \dot{S}_{ij} + \frac{1}{3}\dot{\sigma}_{\alpha\alpha}\,\delta_{ij} \qquad \text{and} \qquad \dot{\sigma}_{\alpha\alpha} \equiv \frac{E}{1-2\nu}\,\dot{\varepsilon}_{\alpha\alpha} \quad . \qquad 2\text{-}11$$

Substituting Eqs. 2-11 into Eq. 2-10, it becomes

$$\dot{\varepsilon}_{ij} = \frac{1+\nu}{E}\dot{S}_{ij} + \frac{1}{3}\dot{\varepsilon}_{\alpha\alpha}\,\delta_{ij} + \frac{9}{4}\frac{S_{kl}\,\dot{S}_{kl}}{\bar{\sigma}^2\,H}\,S_{ij} \quad . \qquad 2\text{-}12$$

Multiply S_{ij} through Eq. 2-12 and summing up, we have

$$S_{ij}\,\dot{\varepsilon}_{ij} = \frac{1+\nu}{E}\,S_{ij}\,\dot{S}_{ij} + \frac{1}{3}\,\dot{\varepsilon}_{\alpha\alpha}\,S_{ij}\,\delta_{ij} + \frac{9}{4}\frac{S_{kl}\,\dot{S}_{kl}}{\bar{\sigma}^2\,H}\,S_{ij}\,S_{ij}, \qquad 2\text{-}13$$

Make use of the identities $S_{ij}\,\delta_{ij} \equiv 0$ and $S_{ij}\,S_{ij} \equiv \frac{2}{3}\bar{\sigma}^2$, Eq. 2-13 can be further simplified to

$$S_{ij}\,\dot{\varepsilon}_{ij} = \frac{1}{2G}\,S_{ij}\,\dot{S}_{ij} + \frac{3}{2H}\,S_{ij}\,\dot{S}_{ij}$$

or

$$S_{ij}\,\dot{S}_{ij} = \frac{2GH}{H+3G}\,S_{ij}\,\dot{\varepsilon}_{ij} \quad , \qquad 2\text{-}14$$

where $G = E/2(1+\nu)$ is the shear modulus. Substitute Eq. 2-14 back into Eq. 2-12 and rearrange it,

$$\dot{S}_{ij} = 2G(\dot{\varepsilon}_{ij} - \frac{1}{3}\dot{\varepsilon}_{\alpha\alpha}\delta_{ij} + Q\, S_{kl}\,\dot{\varepsilon}_{kl}\, S_{ij}) \quad , \qquad 2\text{-}15$$

where $Q = -9G/[2\bar{\sigma}^2(H+3G)]$. Using the previous relations in Eq. 2-11, we have

$$\dot{S}_{ij} = \dot{\sigma}_{ij} - \frac{1}{3}\dot{\sigma}_{\alpha\alpha}\delta_{ij} = \dot{\sigma}_{ij} - \frac{E}{3(1-2\nu)}\dot{\varepsilon}_{\alpha\alpha}\delta_{ij}$$

or

$$\dot{S}_{ij} = \dot{\sigma}_{ij} - \frac{2G}{3}\left(\frac{1+\nu}{1-2\nu}\right)\dot{\varepsilon}_{\alpha\alpha}\delta_{ij} \quad . \qquad 2\text{-}16$$

Inserting Eq. 2-16 into Eq. 2-15, the final form is

$$\dot{\sigma}_{ij} = 2G(\dot{\varepsilon}_{ij} + \frac{\nu}{1-2\nu}\dot{\varepsilon}_{\alpha\alpha}\delta_{ij} + Q\, S_{kl}\,\dot{\varepsilon}_{kl}\, S_{ij}) \quad . \qquad 2\text{-}17$$

We now have completed the formulation of the incremental relationships between the stresses and strains of elastic-plastic solids. A similar derivation has been reported by Yamada, Yoshimura and Sakurai[2].

The general constitutive equations are then reduced below for the analyses of the elastic-plastic flow under the conditions of both plane strain and plane stress cases. Both cases require that the transverse shears vanish and that all dependent variables are functions of the planar coordinates only. It is convenient to develop the equations in matrix form for the finite element calculation. The notation employed is similar to that utilized by Swedlow[1] with indicies i = 1, 2, 3 interpreted as subscripts x, y, z respectively.

2.1 PLANE STRAIN

In the case of plane strain, we assume that $\dot{\varepsilon}_{zz} = \dot{\varepsilon}_{xz} = \dot{\varepsilon}_{yz} = 0$ which give $\dot{\tau}_{xz} = \dot{\tau}_{yz} = 0$. Under these conditions, Eqs. 2-17 can be expressed in matrix form as

$$[\dot{\sigma}] = [D_\varepsilon] \times [\dot{\varepsilon}] \qquad 2\text{-}18$$

where the matrix vectors consisting of the planar components of the incremental stresses and incremental strains are defined as

$$[\dot{\sigma}] = \begin{bmatrix} \dot{\sigma}_{xx} \\ \dot{\sigma}_{yy} \\ \dot{\tau}_{xy} \end{bmatrix} \quad \text{and} \quad [\dot{\varepsilon}] = \begin{bmatrix} \dot{\varepsilon}_{xx} \\ \dot{\varepsilon}_{yy} \\ \dot{\gamma}_{xy} \end{bmatrix} \quad \text{respectively.}$$

Note that the engineering shear strain γ_{xy} is used here in order to keep $[D_\varepsilon]$ symmetrical and hence the later operation in finite element calculation is simplified; whereas tensor notation ε_{xy} is used previously for mathematical convenience. The symmetrical coefficient matrix in plane strain condition is

$$[D_\varepsilon] = \begin{bmatrix} \frac{1-\nu}{1-2\nu} + Q\,S_{xx}^2 & \frac{\nu}{1-2\nu} + Q\,S_{xx}\,S_{yy} & Q\,S_{xx}\,\tau_{xy} \\ & \frac{1-\nu}{1-2\nu} + Q\,S_{yy}^2 & Q\,S_{yy}\,\tau_{xy} \\ \text{sym.} & & \frac{1}{2} + Q\,\tau_{xy}^2 \end{bmatrix} \qquad 2\text{-}19$$

The incremental stress in thickness direction, $\dot{\sigma}_{zz}$, is obtained from the relation of volume dilatation, Eq. 2-11,

$$\dot{\sigma}_{zz} = \frac{E}{1-2\nu}(\dot{\varepsilon}_{xx} + \dot{\varepsilon}_{yy}) - \dot{\sigma}_{xx} - \dot{\sigma}_{yy} \quad . \qquad 2\text{-}20$$

2.2 PLANE STRESS

We define this case by $\dot{\sigma}_{zz} = \dot{\tau}_{xz} = \dot{\tau}_{yz} = 0$ which give $\dot{\varepsilon}_{xz} = \dot{\varepsilon}_{yz} = 0$. Substitute these conditions into Eq. 2-17, we can express the planal stress increments $\dot{\sigma}_{xx}$, $\dot{\sigma}_{yy}$ and $\dot{\tau}_{xy}$ in terms of four strain increments, i.e. $\dot{\varepsilon}_{xx}$, $\dot{\varepsilon}_{yy}$, $\dot{\gamma}_{xy}$ and $\dot{\varepsilon}_{zz}$. However, $\dot{\varepsilon}_{zz}$ can be expressed explicityly in terms of the other three planal components of strain increments by

$$(\frac{1-\nu}{1-2\nu}) + QS_{zz}^2)\dot{\varepsilon}_{zz} + (\frac{\nu}{1-2\nu} + QS_{zz}S_{xx})\dot{\varepsilon}_{xx} + (\frac{\nu}{1-2\nu} + QS_{zz}S_{yy})\dot{\varepsilon}_{yy} + QS_{zz}\tau_{xy}\dot{\gamma}_{xy} =$$

$\frac{\dot{\sigma}_{zz}}{2G} = 0$. The final results relate the three planal stress increments and the three planal strain increment by

$$[\dot{\sigma}] = [D_\sigma] \times [\dot{\varepsilon}] \quad , \tag{2-21}$$

where $[D_\sigma]$ is the coefficient matrix for the plane stress condition

$$[D_\sigma] = \frac{E}{1-\nu^2}\begin{bmatrix} 1-P(S_{xx}+\nu S_{yy})^2 & \nu-P(S_{xx}+\nu S_{yy})(S_{yy}+\nu S_{xx}) & (\nu-1)P(S_{xx}+\nu S_{yy})\tau_{xy} \\ & 1-P(S_{yy}+\nu S_{xx})^2 & (\nu-1)P(S_{yy}+\nu S_{xx})\tau_{xy} \\ \text{Sym.} & & \frac{1-\nu}{2} - (1-\nu)^2 P\tau_{xy}^2 \end{bmatrix} \tag{2-22}$$

and $\frac{1}{P} = S_{xx}^2 + 2\nu\, S_{xx}\, S_{yy} + S_{yy}^2 + 2(1-\nu)\tau_{xy}^2 + \frac{2(1-\nu)H}{9G}\bar{\sigma}^2$. The incremental strain in thickness direction, $\dot{\varepsilon}_{zz}$, can also be calculated from Eq. 2-11

$$\dot{\varepsilon}_{zz} = \frac{1-2\nu}{E}(\dot{\sigma}_{xx} + \dot{\sigma}_{yy}) - \dot{\varepsilon}_{xx} - \dot{\varepsilon}_{yy} \quad . \tag{2-23}$$

2.3 REFERENCES

1. Swedlow, J. L., Williams, M. L. and Yang, W. H., "Elasto-Plastic Stresses and Strains in Cracked Plates," Proceedings of the First International Conference on Fracture, pp. 259-282 (1965).

2. Yamada, Y. and Yoshimura, N. and Sakurai, T., "Plastic Stress-Strain Matrix and its Application for the Solution of Elastic-Plastic Problems by the Finite Element Method," International Journal of Mechanics Science, Vol. 10, pp. 343-354 (1967).

CHAPTER III FINITE ELEMENT METHOD

The finite element method is essentially a generalization of standard structural analysis which permits the calculation of forces and deflections of ordinary framed structures. The method was developed originally in the aircraft industry. Recently, the application of this method is extended into the field of fracture mechanics[1,2].

The basic concept of the finite element method is that a continuum is considered to be an assemblage of elements which are interconnected at a finite number of joints or nodal points. Within each element the displacement components are assumed to vary in such a way that the displacement of any point within the element is determined by the displacements of the nodal points on the boundary of that element. Although the governing matrix equations have been presented elsewhere[3,4], for the sake of completeness, a brief outline of the formulation will be given.

In this analysis, we adopt the simplest first-order triangular elements in which the displacements are taken as linear functions of the spatial coordinates. Figure 3-1 shows a typical triangular element with nodal points i, j, m numbered in counterclockwise order. The nodal point i has coordinates X_i, Y_i, etc. The incremental displacement components $\dot{u}$ and $\dot{v}$, in the x- and y- directions respectively, are assumed to display a linear variation over the element, and they are given by

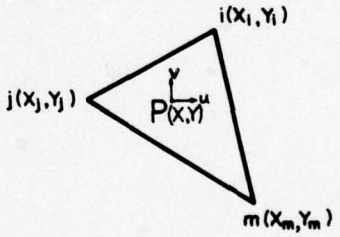


Fig. 3-1

$$\dot{u} = a_1 + a_2 x + a_3 y$$

$$\dot{v} = a_4 + a_5 x + a_6 y \qquad 3\text{-}1$$

The elemental strain increments are then given by

$$[\dot{\varepsilon}] = \begin{bmatrix} \dot{u}_{,x} \\ \dot{v}_{,y} \\ \dot{u}_{,y} + \dot{v}_{,x} \end{bmatrix} = \begin{bmatrix} a_2 \\ a_6 \\ a_3 + a_5 \end{bmatrix} \qquad 3\text{-}2$$

A comma in the subscript denotes partial differentiation. The six constants in Eq. 3-1, a_i's, may be solved in terms of the nodal coordinates and nodal displacement increments. From Eq. 3-2 the strain increments can then be expressed by the matrix relationship

$$[\dot{\varepsilon}] = [B] \times [\dot{u}]/2\Delta \qquad 3\text{-}3$$

where Δ represents the area of the element, [B] is identified by

$$[B] = \begin{bmatrix} y_j - y_m & 0 & y_m - y_i & 0 & y_i - y_j & 0 \\ 0 & x_m - x_j & 0 & x_i - x_m & 0 & x_j - x_i \\ x_m - x_j & y_j - y_m & x_i - x_m & y_m - y_i & x_j - x_i & y_i - y_j \end{bmatrix} \qquad 3\text{-}4$$

and

$$[\dot{u}] = \begin{bmatrix} \dot{u}_i \\ \dot{v}_i \\ \dot{u}_j \\ \dot{v}_j \\ \dot{u}_m \\ \dot{v}_m \end{bmatrix} \qquad 3\text{-}5$$

is the displacement increment vector. It is noted that the matrix [B] is independent of the position within the element, and hence the strains are constant throughout the element. The general incremental form of the stress-strain

relation is

$$[\dot{\sigma}] = [D] \times [\dot{\varepsilon}] \qquad 3\text{-}6$$

as it is discussed in the previous chapter. [D] is replaced by $[D_\varepsilon]$ or $[D_\sigma]$ under the conditions of plane strain or plane stress respectively.

The surface tractions on each element are replaced by statically equivalent nodal forces. The condition of equilibrium at nodal points is satisfied by minimizing the total potential energy of the system. A linear relation between the changes in nodal forces and the nodal displacement increments is followed, having the form

$$[\dot{f}] = [k] \times [\dot{u}] \qquad 3\text{-}7$$

where $[\dot{f}]$ is a column matrix containing the x and y components of the nodal force increments at nodes i, j, and m,

$$[\dot{f}] = \begin{bmatrix} \dot{f}_i^x \\ \dot{f}_i^y \\ \dot{f}_j^x \\ \dot{f}_j^y \\ \dot{f}_m^x \\ \dot{f}_m^y \end{bmatrix} \qquad 3\text{-}8$$

where the superscript x and y denotes the directions of the forces. In Eq. 3-7, [k] is a six-by-six symmetric matrix and is commonly referred to as the elemental stiffness matrix which can be calculated from the relation

$$[k] = [B]^T \times [D] \times [B] \cdot t/4\Delta \qquad 3\text{-}9$$

where the superscript T denotes the matrix transpose and t is the thickness of the element. In the elastic-plastic range, it is clear that [k], being a function of [D], depends on the instantaneous stress state in the element as well as on the elastic constants and element geometry.

When the equilibrium of all elements in the assemblage is considered, the overall stiffness matrix, [K], of the structure can be generated from individual elemental stiffness matrices. The final equilibrium of the structure becomes

$$[K] \times [\dot{U}] = [\dot{F}] \qquad 3\text{-}10$$

where

$$[\dot{F}] = \begin{bmatrix} \dot{F}_1^x \\ \dot{F}_1^y \\ \cdot \\ \cdot \\ \cdot \\ \dot{F}_N^x \\ \dot{F}_N^y \end{bmatrix} \quad \text{and} \quad [\dot{U}] = \begin{bmatrix} \dot{u}_1 \\ \dot{v}_1 \\ \cdot \\ \cdot \\ \cdot \\ \dot{u}_N \\ \dot{v}_N \end{bmatrix}$$

represent the applied force increments at all nodes and the incremental displacement field of the structure respectively, and N is the total number of nodes. The overall stiffness

$$[K] = \Sigma [k] \qquad 3\text{-}11$$

is a square (2N x 2N), symmetric and usually banded matrix.

The incremental displacement field $[\dot{U}]$ resulting from an applied force system $[\dot{F}]$ may be obtained by solving Eq. 3-10. The elemental strain and stress increments are then calculated from Eq. 3-3 and 3-6 respectively.

3.1 DISPLACEMENT BOUNDARY CONDITIONS

In this analysis, displacement boundary conditions are used almost exclusively for two reasons: (1) it is readily available in the case of small scale yielding, and (2) we may use the displacement increments on the boundary as a guide to estimate the incremental strain in each element for a particular loading step. We shall discuss both of these aspects in a later section.

For these specified displacements, the stiffness matrix and the force vector have to be modified in the following manner. The detail of this procedure is explained in Ref. 3.

Let us assume that we have a set of 2N equations,

$$K_{ij}\,\dot{U}_j = \dot{F}_i \qquad i = 1,2, \ldots 2N \tag{3-12}$$

and that we have a displacement component $\dot{U}_{(q)}$ specified to be equal to α. We then precede to modify the force vector such that

$$\dot{F}'_i = \dot{F}_i - K_{i(q)}\alpha \qquad i = 1,2, \ldots 2N \text{ and } i \neq q \tag{3-13}$$

and

$$\dot{F}'_{(q)} = \alpha$$

where $\dot{F}'$ is the modified force vector. Then the corresponding row and column of the stiffness matrix is made zero and the diagonal term is made unity. In the special but common case of $\alpha = 0$, it is only necessary to modify the matrix as described above, leaving the force vector unchanged except for $\dot{F}'_{(q)} = 0$.

3.2 GEOMETRICAL LAYOUT NEAR THE CRACK TIP

In this analysis, the stresses and strains are assumed to be constant throughout each element. Therefore, it is a usual practice to avoid a drastic change of stresses or strains between the neighboring elements. The geometrical layout for the finite element calculation near a crack tip is shown in Fig. 3-2. This particular assembly is chosen such that the ratio of the distance from crack tip to two adjacent nodal points along any radial line is

always kept constant except in the immediate neighborhood of the crack tip. As a consequence, the ratio of the stresses or strains of two neighboring elements is nearly a constant. In addition to that, it is also convenient to study the stress or strain distributions around a crack tip as a function of θ, the angle away from the crack line.

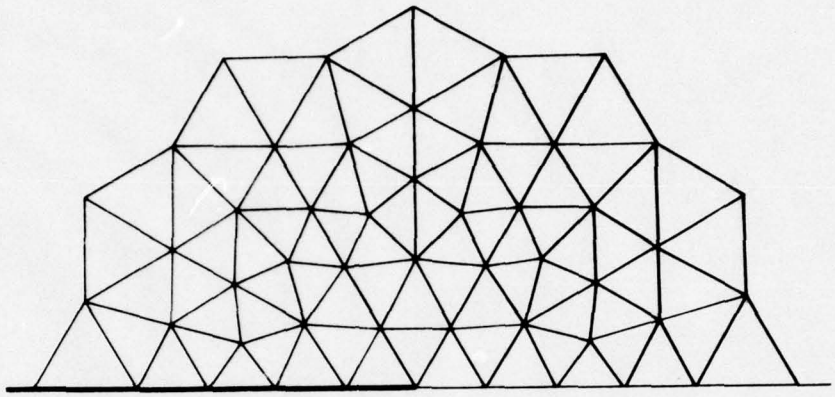


Fig. 4-2 The finite element layout near a crack tip.

3.3 CALCULATION SCHEME

The material characteristic in the plastic region is approximated by the power law

$$\bar{\sigma} = k\bar{\varepsilon}^{N} \qquad 3\text{-}14$$

where N is the strain hardening exponent, k is a constant equal to $E^{N} \cdot \sigma_Y^{1-N}$ and σ_Y is the yield stress of the material. $\bar{\varepsilon}$ is the effective strain defined as

$$\bar{\varepsilon} = \frac{\bar{\sigma}}{E} + \bar{\varepsilon}^{p} \qquad 3\text{-}15$$

In the case of uniaxial tensile loading, $\bar{\sigma}$ and $\bar{\varepsilon}$ are replaced by the true stress and true strain respectively. In the finite element calculation, the infinitesimal deformation theory is employed in each individual loading steps. The

geometry is updated after each increment. This procedure is consistent with the manner in which the true stresses and true strains are obtained.

In the finite element calculation, we approximate the nonlinear behavior of plasticity as piecewise linear within each small loading step. Therefore, the slope of the curve $\bar{\sigma}$ versus $\int \dot{\bar{\varepsilon}}^p$, deonoted by H in Eq. 2-5, is replaced by the slope of a secant connecting two material points on the curve which represent respectively the state of stress before and after the loading step. Since the state of stress after the current loading step is not known, an estimation has to be made.

Assume the effective strain, $\bar{\varepsilon}$, of each element bears a linear relationship with the applied displacement boundary condition, i.e.

$$\delta U \sim \delta \bar{\varepsilon}$$

or

$$\frac{U_+ - U_o}{U_o - U_-} = \frac{\bar{\varepsilon}'_+ - \bar{\varepsilon}_o}{\bar{\varepsilon}_o - \bar{\varepsilon}_-} \qquad 3\text{-}16$$

where U_+, U_o and U_- are respectively the boundary displacements at one step ahead, current step and one step behind. $\bar{\varepsilon}'_+$, $\bar{\varepsilon}_o$ and $\bar{\varepsilon}_-$ are the projected, current and passed effective strains of an element. $\bar{\varepsilon}'_+$ is further modified by the mis-estimate in the effective strain of last loading step,

$$\bar{\varepsilon}_+^{(i)} = \bar{\varepsilon}'_+ - (\bar{\varepsilon}_+^{(i-1)} - \bar{\varepsilon}_o) \qquad 3\text{-}17$$

the quantity in the parathesis is the difference between the estimated effective strain and the effective strain actually calculated after the last loading step. $\bar{\varepsilon}_+^{(i)}$ is the estimated effective strain used to evaluate the secant modulus, H, for the current loading step. The estimated effective plastic strain $\bar{\varepsilon}_+^p$ can be calculated from

$$\bar{\varepsilon}_+^p = \bar{\varepsilon}_+^{(i)} - \frac{\bar{\sigma}_+^{(i)}}{E} \qquad 3\text{-}18$$

where $\bar{\sigma}_+^{(i)}$ is obtained from the relation $\bar{\sigma}_+^{(i)} = k\bar{\varepsilon}_+^{(i)^N}$. The secant modulus is then

$$H = \frac{\bar{\sigma}_+^{(i)} - \bar{\sigma}_o}{\bar{\varepsilon}_+^p - \bar{\varepsilon}_o^p} \qquad 3\text{-}19$$

The current stress and H so obtained for each element are used to evaluate $[D_\varepsilon]$ or $[D_\sigma]$ according to Eq. 2-19 and 2-22. Consequently the elemental stiffness matrices [k] are obtained and the structural stiffness matrix, [K] is followed. After the insertion of boundary condition and solving for the linear system, Eq. 3-10, the incremental displacement field $[\dot{U}]$ corresponding to an incremental force vector $[\dot{F}]$ are obtained. The strain and stress incremental for each element are then calculated from Eq. 3-3 and 3-6 respectively. The incremental effective plastic strain $\Delta\bar{\varepsilon}^p$ is calculated from incremental strain components through Eq. 2-6 and the total effective plastic strain $\bar{\varepsilon}^p$ is simply the sum of $\Delta\bar{\varepsilon}^p$. The sum of stress increments gives the state of stresses of each element. The effective stress of the element is calculated from the stress as it is defined in Eq. 2-6.

It should be noted that the derivative of $\bar{\sigma}$ as expressed in Eq. 2-8

$$\dot{\bar{\sigma}} = \frac{3\, S_{ij}}{2\, \bar{\sigma}}\, \dot{S}_{ij} \qquad 3\text{-}20$$

is not equal to the effective stress increment $\Delta\bar{\sigma}$ defined by

$$\Delta\bar{\sigma} = \left[\frac{3}{2}\,(S_{ij} + \Delta S_{ij})(S_{ij} + \Delta S_{ij})\right]^{1/2} - \bar{\sigma} \qquad 3\text{-}21$$

Rearrange Eq. 3-21 and multiply it by itself,

$$\bar{\sigma}^2 + 2\,\bar{\sigma}\cdot\Delta\bar{\sigma} + (\Delta\bar{\sigma})^2 = \frac{3}{2}\,S_{ij}\,S_{ij} + 3\,S_{ij}\,\Delta S_{ij} + \frac{3}{2}\,\Delta S_{ij}\,\Delta S_{ij} \qquad 3\text{-}22$$

Note that $\bar{\sigma}^2 = \frac{3}{2}\,S_{ij}\,S_{ij}$, $\Delta\bar{\sigma}$ can then be expressed by

$$\Delta\bar{\sigma} = \frac{3\,S_{ij}}{2\,\bar{\sigma}}\,\Delta S_{ij} + \frac{1}{2\bar{\sigma}}\left[\frac{3}{2}\,\Delta S_{ij}\,\Delta S_{ij} - (\Delta\bar{\sigma})^2\right] \qquad 3\text{-}23$$

Comparing Eq. 3-20 and Eq. 3-23, it is clear that the difference between $\dot{\bar{\sigma}}$ and $\Delta\bar{\sigma}$ are of the second order of ΔS_{ij}. Hence, using Eq. 3-21 in the finite element formulation is justified by keeping loading step small such that ΔS_{ij} is small in comparison with $\bar{\sigma}$.

3.4 REFERENCES

1. Swedlow, J. L., "The Thickness Effect and Plastic Flow in Cracked Plates," Ph.D. Dissertation, California Institute of Technology (1965).

2. Chan, S. K., Tuba, I. S. and Wilson, W. K., "On the Finite Element Method on Linear Fracture Mechanics," Engineering Fracture Mechanics, Vol. 2, pp. 7-17 (1970).

3. Zienkiewicz, O. C., "The Finite Element Method in Engineering Science," McGraw-Hill, London (1971).

4. Marcal, P. V. and King, I. P., "Elastic-Plastic Analysis of Two-dimensional Stress Systems by the Finite Element Method," International Journal of Mechanics Science, Vol. 9, pp. 143-155 (1967).

CHAPTER IV COMPARISON OF FEM CALCULATION AND EXPERIMENTAL MEASUREMENTS

4.1 PLANE STRESS CALCULATION

Plane stress calculations are made for two batches of aluminum alloy. The Young's modulus, E, and the Poisson's ratio, ν, are 11×10^3 ksi and 0.34 respectively. The uniaxial tensile stress-strain curves of these two batches of aluminum alloys are shown in Fig. 4-1. The yield stress, σ_Y, is 7.26 ksi, and the strain hardening exponent, N, is 0.315 for batch C aluminum alloy. Whereas for batch B aluminum alloy the yield stress and the strain hardening exponent are 10 ksi and 0.22 respectively. In the finite element calculation, the stress-strain relations are approximated by

$$\sigma = E\varepsilon \qquad \text{for} \qquad \sigma \leq \sigma_Y \quad , \qquad 4\text{-}1a$$

and

$$\sigma = k\varepsilon^N \qquad \text{for} \qquad \sigma \geq \sigma_Y \qquad 4\text{-}1b$$

where $k = E^N \sigma_Y^{1-N}$. These relations represent a good material characterization

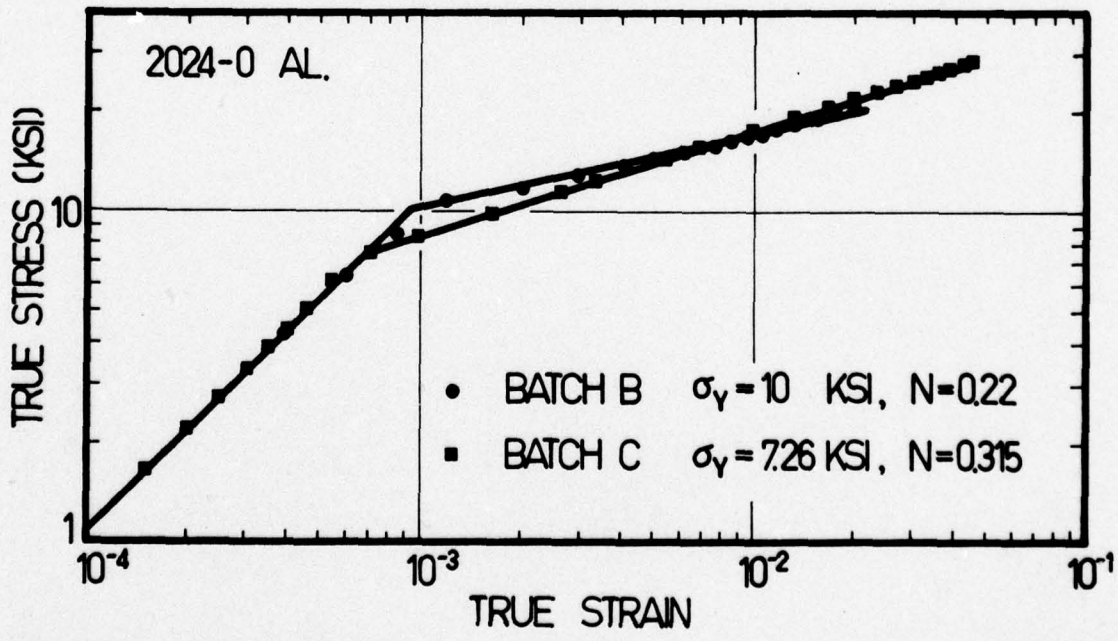


Fig. 4-1 Uniaxial tensile stress-strain curves for 2024-0 aluminum alloys, batch B and C.

as shown in Fig. 4-1.

The results of the calculations are compared with the moire strain measurements made by Gavigan, Ke and Liu[1]. The measurements were made on four and eight inches wide, double-edge-notched (DEN) specimens of 0.125, 0.25 and 0.5 inches thick. It should be noted here that the measurements were made for three batches of aluminum alloys, where the values of σ_Y and N of batch A and batch C aluminum are very close to each other. Hence, the calculated results of batch C aluminum are compared with the measurements from both batch A and batch C aluminum specimens.

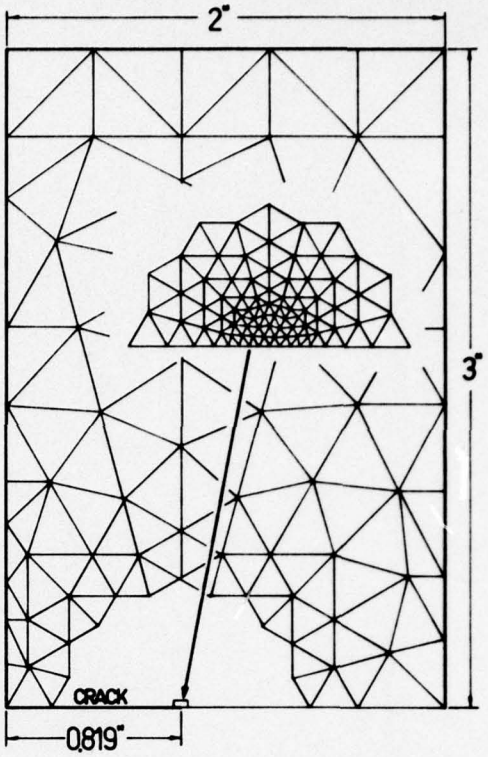


Fig. 4-2 The finite element representation of first quadrant of the DEN specimen. The details of elements near crack tip is inserted.

Fig. 4-2 shows a finite element representation of the first quadrant of the double-edge-notched plate. The mesh is composed of 265 nodes and 468 linear displacement triangular elements. The dimension of the element closest to the crack tip is 0.0035 inches. All the results presented in this study are relatively far away from the crack tip in comparison with the smallest element size. A calculation with a finer mesh was also made. The results are the same. At the far end of the sample, a uniform displacement is applied as the excitation parameter.

Figs. 4-3 show the comparison of calculated and measured y-direction strain, ε_{yy}, distributions along the crack line at different loading levels. The loading level is indicated by the parameter $\Delta/W\varepsilon_Y$, where W is the specimen width, ε_Y is the yield strain and Δ is the elongation measurement made over a gage length of seven inches. The vertical dimension of the finite element representation of the sample used for this calculation, as seen in Fig. 4-2 is three

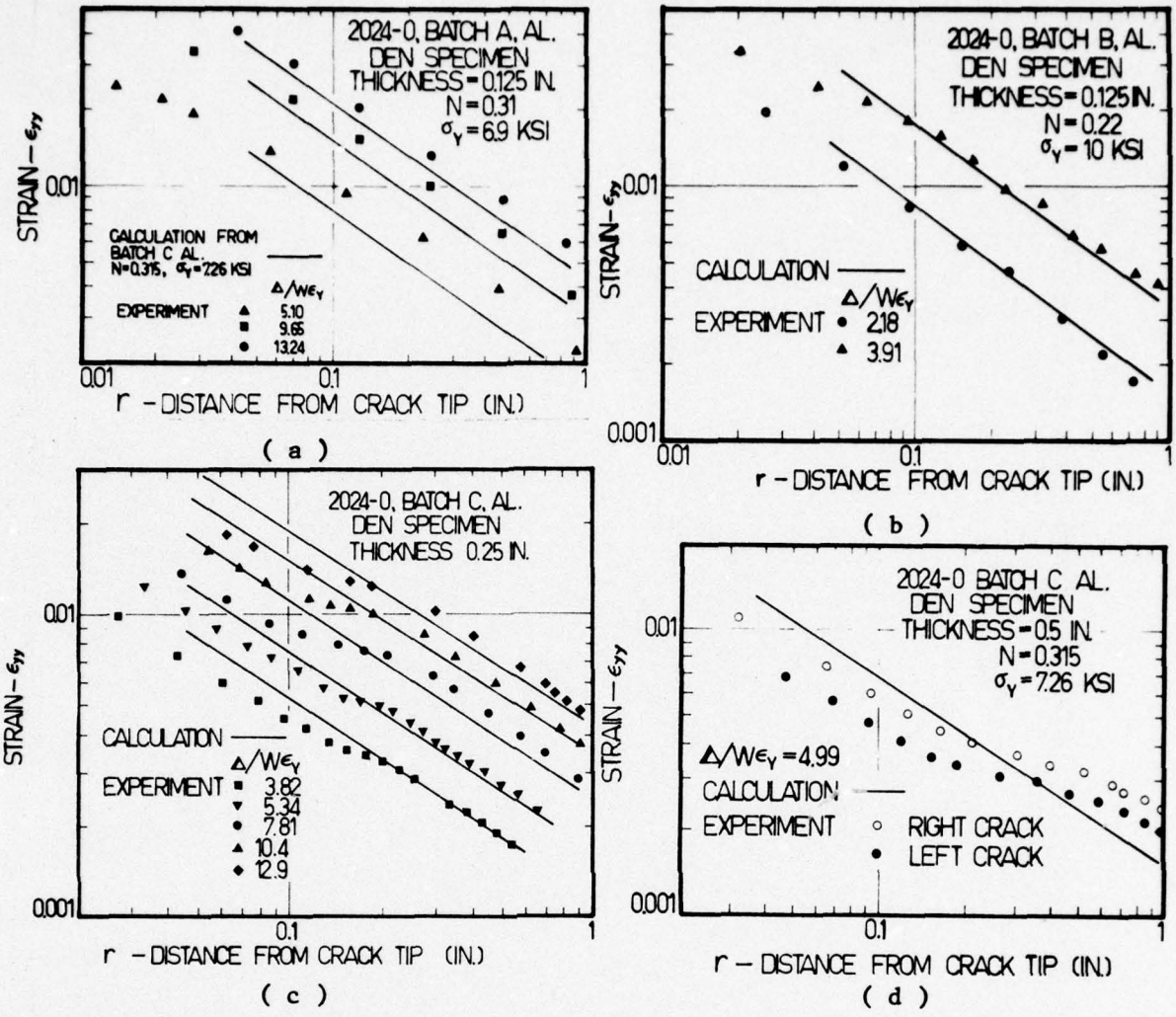


Fig. 4-3 Comparison of calculated ε_{yy} versus the experimental measurements for DEN, 2024-0 aluminum alloys.

inches, which corresponds to a gage length of six inches. Therefore, the average strain of the top most elements were added to make up the total calculated elongation. The corresponding material and specimen thickness are noted on each individual plots. The two sets of experimental points for the two cracks of the same DEN specimen at the same overall elongation of the specimen are shown in Fig. 4-3d. The difference of these two sets of measurements is possibly caused by the internal cracking and by a slight bending. All the comparisons are made in the region of general yielding.

The agreement between the measured and calculated strains in the region

more than about one thickness ahead of the crack tip, i.e. r > t is very good. Whereas in the near tip region the measured strains are less than the calculated ones which reflects the thickness effect introduced by the presence of the crack. It is reasonable to assume that the strains are uniform throughout the thickness of the specimen only in the region where r > t. In this region, the deformation is characterized by plane stress analysis. The slope of the logarithmic plot in the region are 0.75 and 0.70 for batch B and C aluminum alloy respectively, which are close to the values given by the analytical calculations of Rice and Rosengren[2] and Hutchinson,[3] i.e. 0.82 and 0.76 respectively. This comparison suggests that plane stress finite element calculation can be used to characterize the deformation field in the region one thickness away from the crack tip for a DEN specimen in general yielding.

4.2 THREE DIMENSIONAL CHARACTERISTICS OF CRACK TIP DEFORMATION

The plane stress analysis is only an idealized model. The stresses and strains near the crack tip of a plate are in reality much more complicated. The region closer to a crack tip has higher strains and tends to contract more in the thickness direction. But the crack tip region is constrained from thickness contraction by the region of lower strains further away from the crack tip. This constraint induces the tensile stress in the direction of plate thickness, σ_{zz}. Along the crack front and in the interior of a very thick plate, the thickness contraction is negligibly small, and the state of deformation there approaches that of plane strain. On the plate surface, the traction is zero; therefore, the conditions of plane stress prevail. For a cracked thick plate, the state of stresses and strains changes gradually, from that of plane stress on the specimen surface to that of plane strain in the interior. This is true if the plastic zone size is small enough in comparison to the plate thickness.

It is also clear that the rate of transition from the state of plane stress on the surface to the state of plane strain in the interior depends upon the

strain gradient induced from geometrical irregularities. If the gradient is high, the transition is fast; conversely, if the gradient is low, the transition is slow. If there is no strain gradient in the plane of a plate, there is no constraint from the deformation in the plate thickness direction to induce σ_{zz} regardless of how thick the plate is. Close to a crack tip, the strain gradient is steep, and the rate of transition is fast. As the distance from crack tip increases, the strain gradient decreases, and the thickness of the transition layer increases. Far away from the crack tip, the state of stresses and strains throughout the plate thickness is essentially that of plane stress.

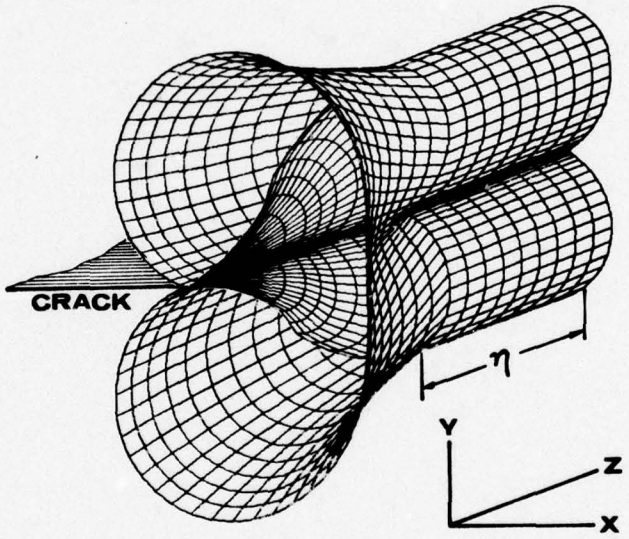


Fig. 4-4 Schematic diagram showing half of the plastic zone. The plane strain plastic zone is imbedded.

A schematic picture of the plastic zone in a thick plate near a crack tip is shown in Fig. 4-4. The size and shape of the plastic zones are approximated by the use of the crack tip stress equation for an elastic medium under either plane stress or plane strain conditions. The zone is taken as the

locus of points at which the von Mises' yield criterion would be exceeded if the elastic stress distribution were unaffected by yielding. Poisson's ratio equal to 0.34 is used in this approximation. If a plate is thick enough, the size of the plane strain zone starts from zero on the plate surface and grows to the fully developed size in the interior. There is a transition region between the plane stress region on the plate surface and the plane strain region in the interior of a thick plate. The difference between the plane stress (on the surface) and plane strain (in the interior) zones indicate the significant effect of lateral constraint on the plastic flow at the crack tip. In the interior of a thick plate, the plane strain plastic zone, $r_{p\varepsilon}$, coincides with r_p. Close to the plate surface, r_p becomes bigger, but $r_{p\varepsilon}$ becomes smaller. The length of the fully developed plane strain region, 2η, relative to the size of the transition region, depends upon the size of the plastic zone relative to the plate thickness. For a thicker plate and for a smaller r_p, η is longer. Within the transition region and the plane strain plastic region, the hydrostatic tensile stress, i.e. $(\sigma_{xx} + \sigma_{yy} + \sigma_{zz})/3$, increases and the effective stress decreases, thereby reducing the overall plastic deformation. It can be said that the crack tip region is "stiffened" against plastic deformation.

In the case of small scale yielding, the size of the plane strain zone depends upon the quantity $(K/\sigma_Y)^2/t$. For a valid K_{Ic} test, the value of the quantity must be less than 0.4, i.e. at this value, an effective plane strain zone exists for the fracture test. At a higher value of this quantity, the stiffening effect is less. In the region of general yielding, the stiffening effect is greatly reduced.

It can be concluded that the crack tip region is stiffened by the triaxial state of stress in the interior of the plate. The stiffened region in the interior restrains the plastic deformation on the surface. Even though the state of stress on the surface is that of plane stress, the measure strains

in this region are much less than those strain values calculated under the plane stress condition.

Ke[4] had made strain measurements on specimens made of other materials at various thicknesses. All their results clearly show the changes of the slope in a log-log plot of strain in loading direction against the distance from the crack tip at two points along the crack line. One takes place at t/2, the other at t, where t is the specimen thickness. The measurements seems to suggest that the stiffened zone extends from the crack tip to a distance equal to the half of the specimen thickness and the effect of stiffening on the surface strain stretches to the region one thickness away from the crack tip.

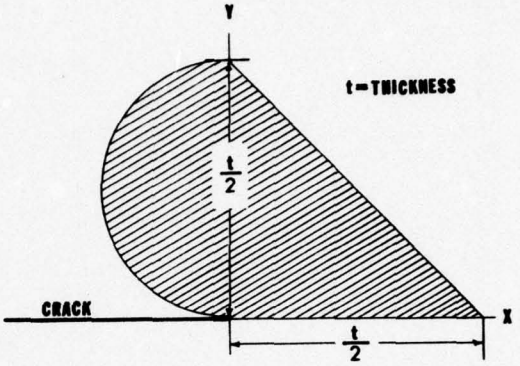


Fig. 4-5 The region of modification within which the stiffness matrix of each element is modified.

4.3 COMPOSITE CALCULATION

With the discussion given in the foregoing section, we proceed to modify the stiffness matrices of the elements close to the crack tip. Fig. 4-5 shows the modification zone within which the stiffness matrix of each element is modified to reflect the stiffening effect of the plane strain plastic zone. The modification zone in both x- and y- directions extends to the half of the specimen thickness. It is assumed that the degree of stiffening is equivalent to a certain size of the "plane strain zone" in the crack tip region. For the sake of simplicity and because of the lack of information, it is further assumed that the shape and the size of this modification zone remains the same throughout the loading process.

For each of the elements within the modification zone, a linear combination of $[D_\sigma]$ and $[D_\varepsilon]$ replaces $[D_\sigma]$. This composite matrix [D] is assumed as

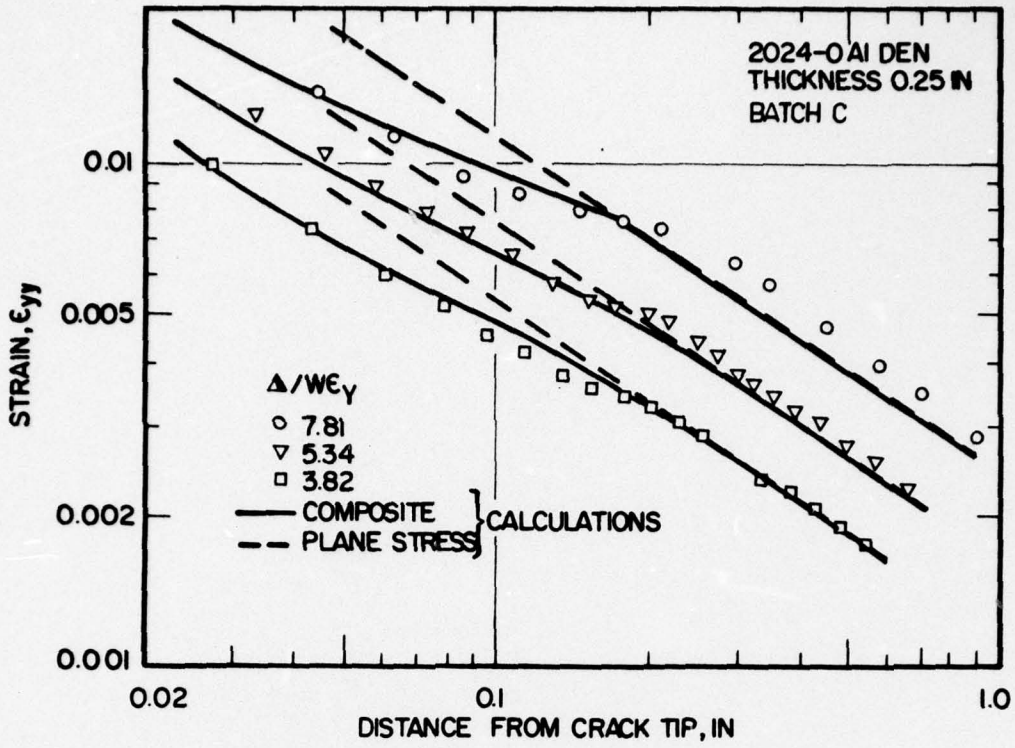
$$[D] = \Omega[D_\varepsilon] + (1 - \Omega)[D_\alpha] \quad , \qquad 4\text{-}2$$

where $[D_\varepsilon]$ and $[D_\sigma]$ are defined respectively in Eq. 2-19 and 2-22 and Ω is the mixing parameter whose value changes linearly with the distance from the crack tip. Outside of the modification zone [D] is equal to $[D_\sigma]$. [D] is thus used to construct the elemental stiffness matrix. For each element inside the modification zone, the strain increment in z-direction is reduced to

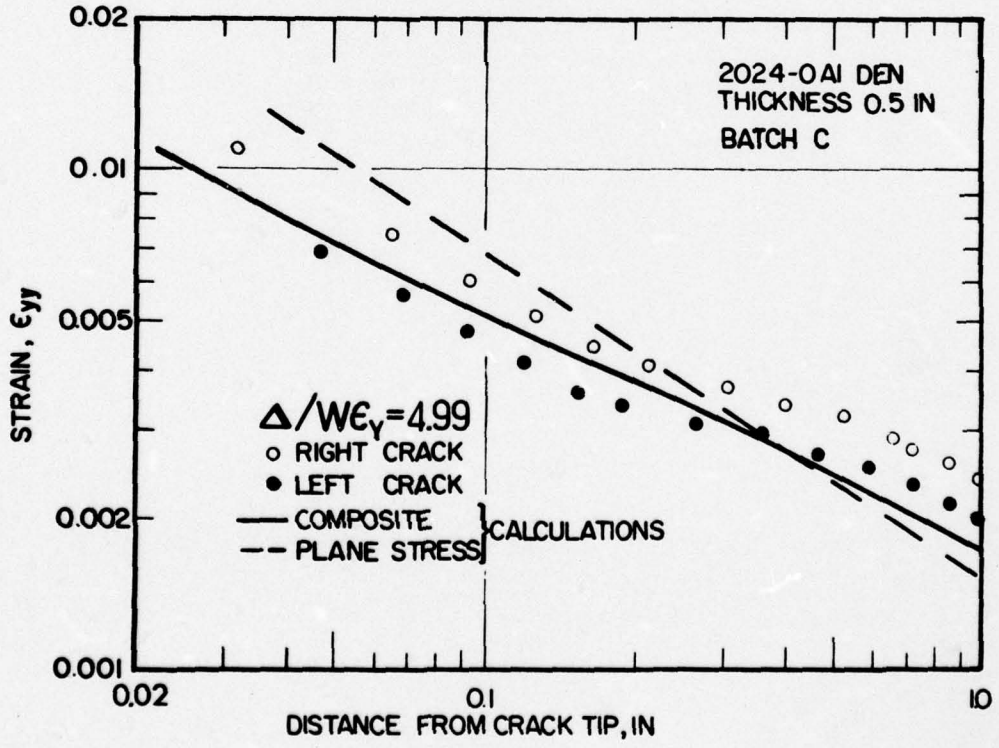
$$\dot{\varepsilon}_{zz} = (1 - \Omega)[\frac{1 - 2\nu}{E}(\dot{\sigma}_{xx} + \dot{\sigma}_{yy}) - \dot{\varepsilon}_{xx} - \dot{\varepsilon}_{yy}] \qquad 4\text{-}3$$

For each element in this zone there are two sets of stress increments, one for plane stress and one for plane strain. These two sets of stress increments could be obtained from the strain increments following Eq. 3-6. The resulting stresses are then used to generate separately the $[D_\sigma]$ and $[D_\varepsilon]$ for the next loading step.

Calculations with composite matrix are made for batch C aluminum alloy at two different thicknesses. The values of Ω are determined by trial and error so as to make the calculated strains, ε_{yy}, match with the measurements. For the 0.25 inch thick plate, the value of Ω changes from 0.04 at the crack tip to zero at the boundary of the modification zone. The value of Ω for the 0.5 inch thick plate is 0.08 at the crack tip. Figs. 4-6 show the results of the composite mode calculation as denoted by the solid lines, whereas the dashed lines represent the plane stress calculation. It is to our surprise that a very small plane strain state could make such a significant change in ε_{yy}. It should be recognized that the composite mode calculation is not intended as an exact three dimensional calculation for the crack tip stresses and strains. The degree of the crack tip stiffening is adjusted by trial and error to fit the experimental data. The purpose of the calculation is to qualitatively show the extent of



(a)



(b)

Fig. 4-6 Near tip strain measurements and calculations, 2024-0 aluminum alloy, batch C.

the three dimensional effect.

One of the important results of the calculation is to reveal that the extent of the plane strain plastic zone is very limited for a specimen loaded considerably into the region of general yielding. For example, for the 0.25 inch thick specimen, in the composite finite element calculation, the value of Ω is only 0.04. This can be interpreted as meaning that the equivalent plane strain plastic zone at the crack tip is only four percent of the plate thickness. However, this is not to say that the actual length of the plane strain zone is four percent of the crack front. Rather, it means that the build up of the triaxial state of stresses and the restraining of plastic deformation at the crack tip are equivalent to a four percent plane strain zone. Hence, it is doubtful that in the 0.25 inch thick plate at these load levels, the true plane strain condition exists at the crack tip. This observation casts a serious doubt on the premise that a small specimen can be used to measure plane strain fracture toughness for a very ductile and tough material.

In Fig. 4-6b, the measurements and the calculated strains of a 0.5 inch thick plate are shown. In the crack tip stiffened region, the calculated strains agree well with the measurements. The intermediate region between the stiffened region and the plane stress region extends to r approximately equals to 0.5 inch, where r denotes the distance from the crack tip. The total ligament, (W-2a), of the specimen is only 2.4 inches. As a consequence, the plane stress region is not large enough to show the characteristic slope of the strain curve as it is in the case of 0.25 inch thick specimen. The results in Figs. 4-6 lead us to conclude that in order to assure a plane stress region in an experiment, the total ligament of a DEN specimen should be ten times or more than the specimen thickness. If a bending load exists such as in the case of a wedge opening load (WOL) type specimen, the ligament should be even wider. It is also clear, that in the case of small scale yielding, in order to observe the characteristic slope of a plane stress plastic zone, the size

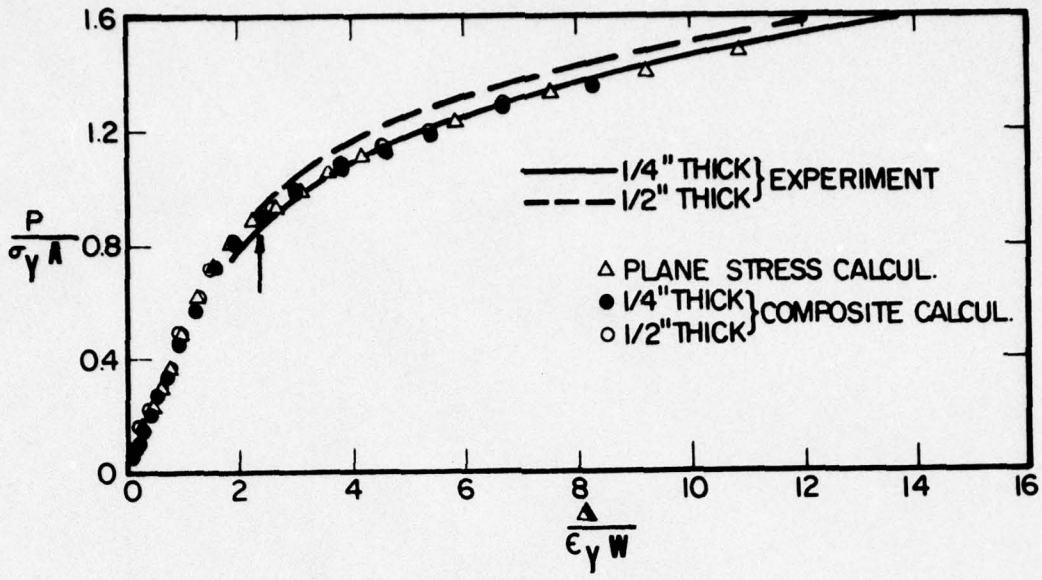


Fig. 4-7 The load-elongation curves of both the pure plane stress calculation and the composite calculations as compared with the experiment data.

of the plastic zone should also be five times or more than the thickness.

If the ligament is wide enough, the crack tip stiffening zone is imbedded in the characteristic plane stress zone. The maximum tensile stress in the stiffening zone is increased above that of the plane stress calculation and the deformation, on the other hand, is reduced. The stiffening effect is strongly controlled by the plate thickness. Therefore, the results of the measurements and the calculations suggest that for the specimens of the same thickness with the same stress and strain fields in the characteristic plane stress zones, the stresses and strains in the stiffened zones must be the same, even though the values of these stresses and strains in the stiffened zone are unknown.

Fig. 4-7 compares the load-elongation curves of both pure plane stress calculation and the composite mode calculation for both 0.25 and 0.5 inch thick specimens with the experimental data of batch C alluminum alloy. The good agreement of these curves with the measurements indicates that the major part of the specimen is under the condition of plane stress. The experimental load-elongation curve of the 0.5 inch thick specimen is only ten percent

higher than the calculated plane stress curve. Although the near tip stress and strain distribution is affected considerably by the crack tip stiffening, but the overall compliances of the specimen have not changed much. The comparison also suggests that the extent of the plane strain zone is very limited.

4.4 REFERENCES

1. Gavigan, W. J., Liu, H. W. and Ke, J. S., "Local and Gross Deformation in Cracked Metallic Plates and an Engineering Ductile Fracture Analysis," ASME Paper 71-PVP-52 (1971).

2. Rice, J. R. and Rosengren, G. F., "Plane Strain Deformation Near a Crack Tip in a Power-Law Hardening Material," J. of Mech. and Phys. of Solids, Vol. 16, p. 1 (1968).

3. Hutchinson, J. W., "Singular Behavior at the End of a Tensile Crack in a Hardening Material," J. of Mech. and Phys. of Solids, Vol. 16, p. 13 (1968).

4. Ke, J. S. "Crack Tip Deformation and Ductile Fracture Criteria," Ph.D. Dissertation, Syracuse University (1974).

CHAPTER V CHARACTERIZATION OF CRACK TIP STRESSES AND STRAINS

From the point of view of continuum mechanics, the stress and strain distributions ahead of a crack could be divided into four regions as illustrated in Fig. 5-1. Region I extends from the crack tip to a distance approximately equal to the half of the specimen thickness. In this region, the plane strain stiffening effect exists and the three dimensional behaviour is prominent. In Region II, the plane stress condition is generally applied. The dominant singularities of both stresses and strains as the variation of the distance from the crack tip, r, approaches to the analytic works by Hutchinson,[1] Rice and Rosengren.[2] Region III lies further away from the crack tip where the material deforms elastically and the stresses and strains change inversely with the square root of the distance from the crack tip. Still further away is region IV where the effects of specimen geometry and the type of loading dominate the deformation

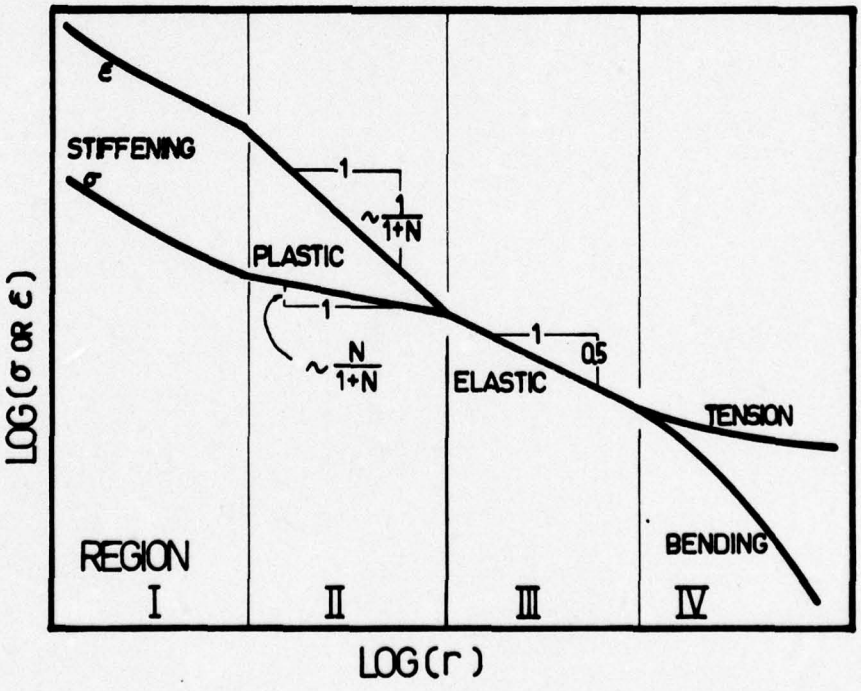


Fig. 5-1 Schematic plot of stress and strain distributions ahead a crack in logarithmic scale.

characteristics. It should be noted that in general not all of this four regions are present. For example, the region III diminishes with increasing load and finally disappears when the load is beyond the general yielding. For a very thick single-edge-cracked specimen, only region I and region IV may exist.

The nature of the plane strain stiffening effect has been discussed in the previous chapter. This chapter will focus our interest in the stress and strain distribution in region II and region III. As it has been shown earlier, the remarkable agreement between the measurement and calculation in region II suggests that the major portion of the specimen is under plane stress condition. The characteristic singularities in this region are close to those predicted by the deformation theory of plasticity.

5.1 SMALL SCALE YIELDING

In order to investigate the characteristics of both region II and region III, plane stress finite element calculations are made in the case of small scale yielding. The materials treated are 2024-0 aluminum alloy, batch B and batch C. In order to avoid redundance only the results from batch C alloy are given. However, the essential results deduced from the calculation of batch B alloy will be provided at the appropriate point. The calculations are made on a semicircular region with displacement boundary conditions. The element layout is shown in Figure 5-2 and the displacement boundary conditions are specified by the elastic solution

$$u = \frac{K_I}{E}\sqrt{\frac{2r}{\pi}}\,\mathrm{Cos}\,\frac{\theta}{2}\left[1 - \nu + (1+\nu)\,\mathrm{Sin}^2\,\frac{\theta}{2}\right]$$

$$v = \frac{K_I}{E}\sqrt{\frac{2r}{\pi}}\,\mathrm{Sin}\,\frac{\theta}{2}\left[1 - \nu - (1+\nu)\,\mathrm{Cos}^2\,\frac{\theta}{2}\right] \qquad 5\text{-}1$$

This particular mesh geometry was discussed in more detail by Tracey,[3] Larsson and Carlsson.[4] The imposed stress intensity factor, K_I in Eq. 5-1 ranges from

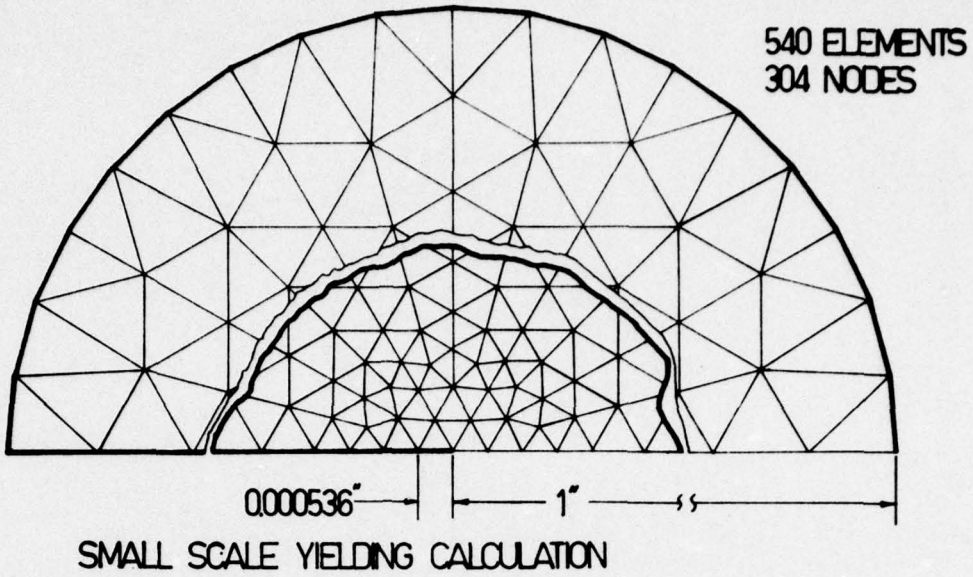


Fig. 5-2 Element layout for small scale yielding calculations.

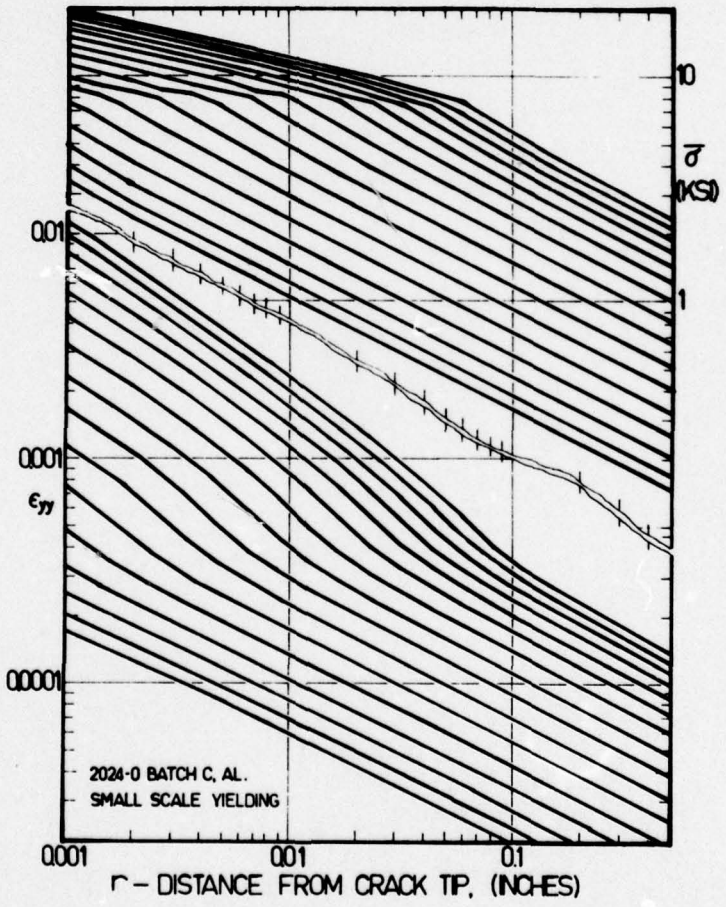


Fig. 5-3 Calculated $\bar{\sigma}$ and ϵ_{yy} for batch C aluminum along the crack line in small scale yielding case.

0.25 to 4.00 ksi$\sqrt{in.}$ Sixteen loading steps are calculated.

The calculated effective stress, $\bar{\sigma}$ and strain in loading direction, ε_{yy}, for batch C aluminum along the crack line are shown in Fig. 5-3. All the other pertinent components; such as σ_{yy}, ε_{xx}, σ_{xx} and $\bar{\varepsilon}^p$, follow a similar pattern. The first load is purely elastic which can be readily identified by the characteristic - 1/2 slopes in the figure. The number of plastically deformed element along the crack line increases with the load. The slopes in the plastically deformed region (region II) is 0.26 for the plot of effective stress and 0.76 for the plot of ε_{yy}. The plastic zone size along the crack line, r_p, can be obtained by extrapolating the plastic portion of the effective stress curve to the point where the effective stress is equal to the yield stress. The detailed crack line stress and strain distributions for this material are shown in the dimensionless plots in Fig. 5-4. The stresses and strains are normalized by the yield stress and yield strain respectively. The distance from the crack tip is normalized by the plastic zone size along the crack line at each individual loading step. Only the last nine loading steps are shown where the value of K_I ranges from 1.125 to 4 ksi$\sqrt{in}$. Each symbol denotes one loading level. In this figure, the characteristic plane stress plastic region (region II) and the characteristic elastic region (region III) are clearly shown.

To the left of $r/r_p = 1$, the y-direction strain and stress can be expressed as

$$\varepsilon_{yy} = \varepsilon_{yy(r=r_p)} \left(\frac{r}{r_p}\right)^{-m} \quad , \quad \text{and} \quad \sigma_{yy} = \sigma_{yy(r=r_p)} \left(\frac{r}{r_p}\right)^{-m'} \qquad 5\text{-}2$$

where $\varepsilon_{yy(r=r_p)}$ and $\sigma_{yy(r=r_p)}$ are the values of ε_{yy} and σ_{yy} at $r = r_p$, and m and m' are constant equal to 0.76 and 0.26 respectively. It is interesting to note that $m + m' \simeq 1$ as it is indicated by Eq. 1-3. In the case of small scale yielding, r_p is related to stress intensity factor by

$$r_p = \alpha \left(\frac{K_I}{\sigma_Y}\right)^2 \qquad 5\text{-}3$$

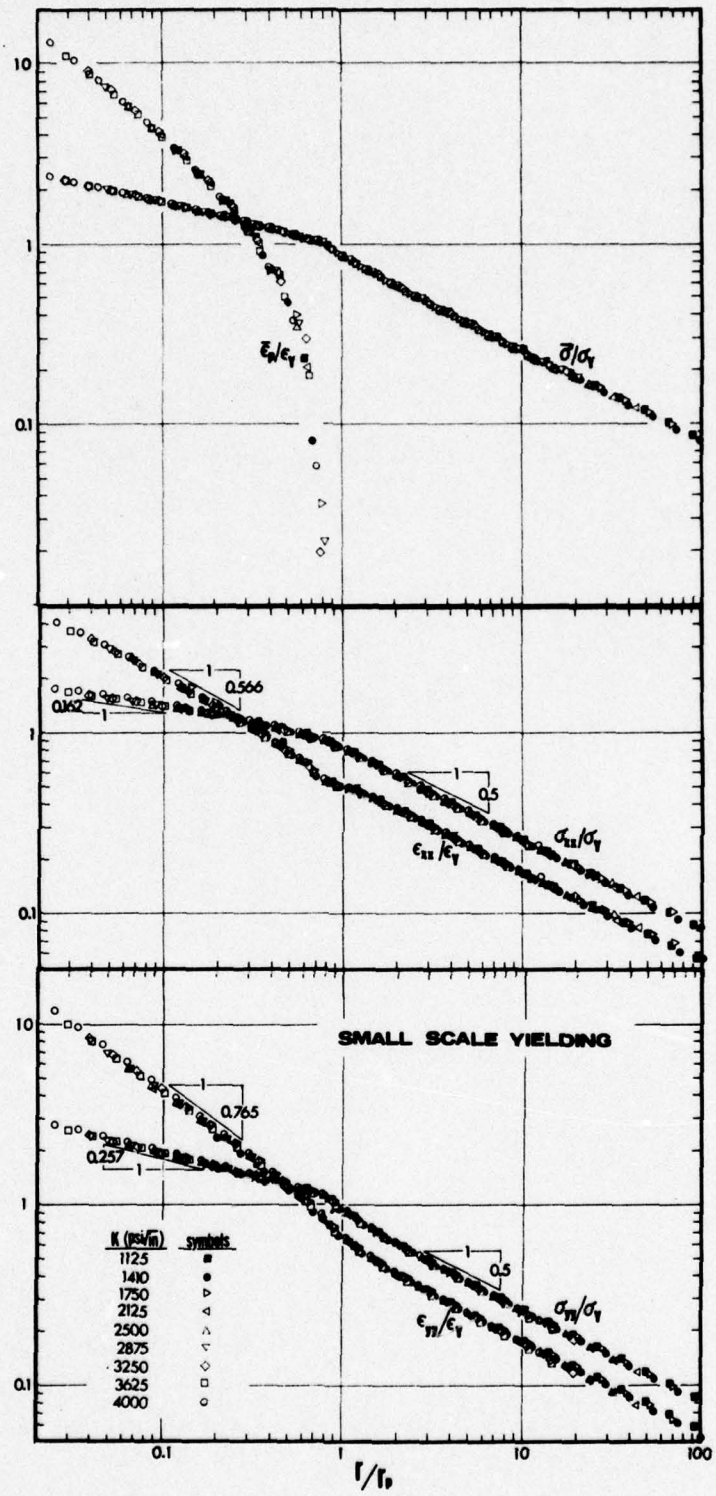


Fig. 5-4 Normalized plots of crack line stresses and strains.

In addition

$$\varepsilon_{yy(r=r_p)} = \frac{\varepsilon_Y}{\beta} \quad , \quad \text{and} \quad \sigma_{yy(r=r_p)} = \frac{\sigma_Y}{\beta'} \qquad 5\text{-}4$$

where ε_Y and σ_Y are yield strain and yield stress of the material respectively. Combining Eqs. 5-2, 5-3 and 5-4, one has the following relations

$$\varepsilon_{yy} = \frac{K_\varepsilon}{r^m} \quad ; \quad \text{and} \quad \sigma_{yy} = \frac{K_\sigma}{r^{m'}}, \qquad 5\text{-}5a$$

where

$$K_\varepsilon = (\frac{\varepsilon_Y}{\beta})\alpha^m(\frac{K_I}{\sigma_Y})^{2m} \quad ; \quad \text{and} \quad K_\sigma = (\frac{\sigma_Y}{\beta'})\alpha^{m'}(\frac{K_I}{\sigma_Y})^{2m'} \qquad 5\text{-}5b$$

K_ε and K_σ can be considered as the strengths of the crack tip strain and stress singularities. Similar relations can also be obtained for σ_{yy}, ε_{xx}, $\bar{\sigma}$ and $\bar{\varepsilon}^p$. The values of β, β' and α can be obtained from the small scale yielding calculation. For batch C aluminum, these values are respectively 1.405, 0.983 and 0.243; whereas for batch B aluminum, the values are 1.353, 0.923 and 0.281.

It is interesting to note that in the case of small scale yielding, the K_I values could also be obtained from the stress and strain distribution of the elastically deformed region (region III) by the following relations

$$K_I = \sqrt{2\pi r}\ \sigma_{yy} \qquad 5\text{-}6$$

$$K_I = \sqrt{2\pi r}\ \sigma_{xx} \qquad 5\text{-}7$$

$$K_I = \frac{E}{1-\nu}\sqrt{2\pi r}\ \varepsilon_{yy} \qquad 5\text{-}8$$

$$K_I = \frac{E}{1-\nu}\sqrt{2\pi r}\ \varepsilon_{xx} \qquad 5\text{-}9$$

The percent of the deviation of the K_I values obtained this way from the imposed

K_I values are 4.20, 0.88, 5.85 and - 1.11% for Eqs. 5-6, 5-7, 5-8 and 5-9 respectively.

5.2 GENERAL YIELDING

Fig. 5-5 shows the results of the plane stress calculation of double-edge-notched (DEN) specimen made of batch C aluminum in general yielding. In addition to the crack line results, the y-direction stress and strain distributions along radial lines 45^o, 60^o and 90^o away from the crack line are shown. The results are plotted in the same manner as Fig. 5-4 and the corresponding plots for small scale yielding are also presented for comparison. The values of r_p for these plots are obtained by the linear extrapolation of effective stress, $\bar{\sigma}$, to yield stress σ_Y in a logarithmic plot of $\bar{\sigma}$ vs. r. The calculated $\bar{\sigma}$ and effective plastic strain, $\bar{\varepsilon}^p$, are also shown and compared in Fig. 5-6.

Plane stress calculation is also made for single-edge-notched (SEN) specimen made of the same material loaded into the region of general yielding. The results are shown in Fig.5-7. The plane stress characteristic region (region II) is clearly shown.

The excellent correlation in the characteristic plane stress region between the both general yielding cases (DEN and SEN) and the case of small scale yielding indicates that a single parameter like r_p is sufficient to characterize the crack tip stresses and strains. Furthermore, the near tip stress or strain in a small sample in general yielding can be used to obtain the equivalent K_I value of a large specimen where the condition of small scale yielding is satisfied. Consider two specimens of same thickness, one large and one small. Both are loaded to the level such that at certain distance from crack tip, r, the y-direction stress or strain is the same in both specimens. The large specimen is wide enough such that the condition of small scale yielding is retained. Hence, the crack tip stresses and strains are characterized by the value of stress intensity factor which is given by the elastic solution. Whereas the second specimen is so small that the state of deformation is general yielding.

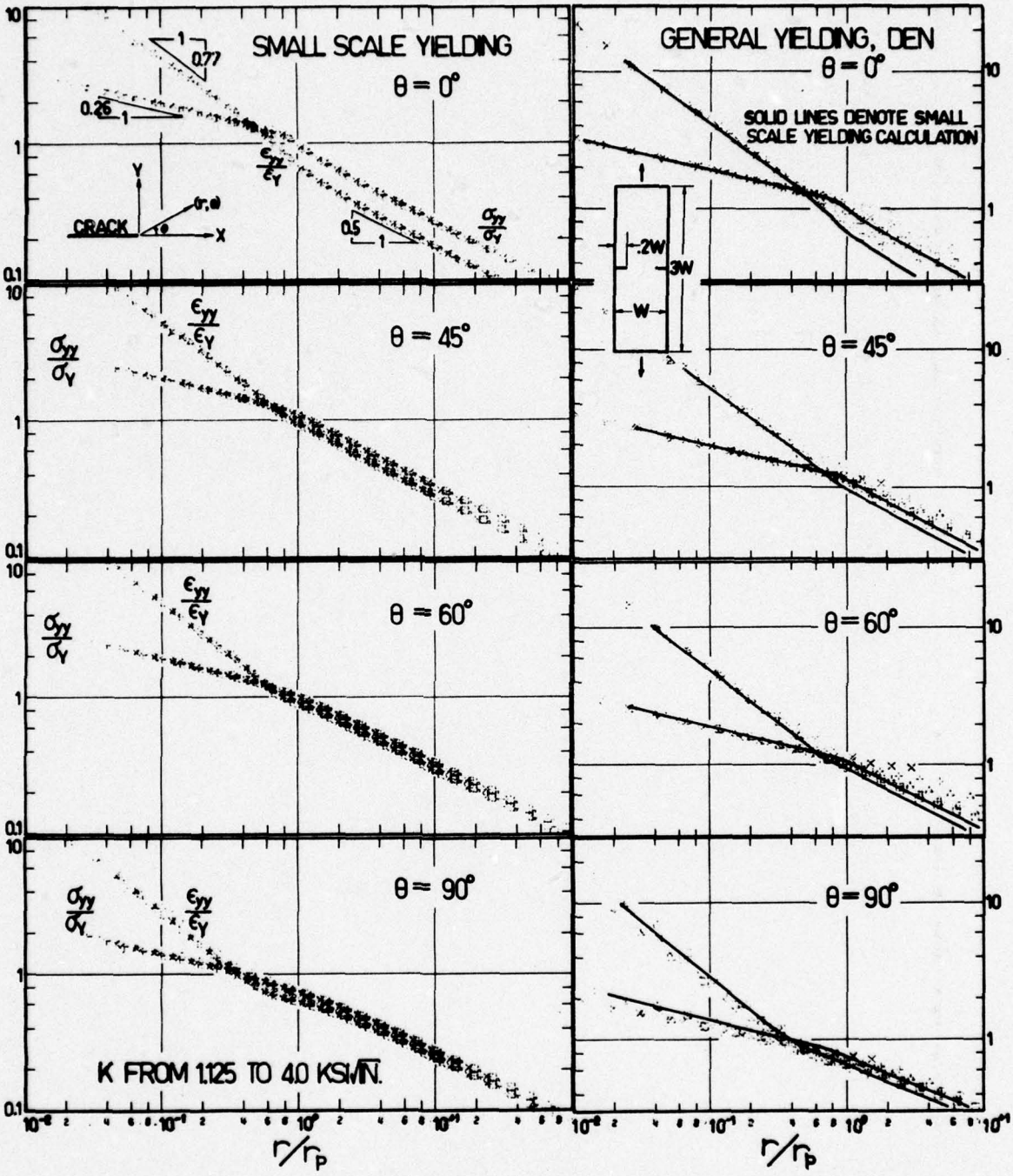


Fig. 5-5 Correlations of near tip stresses and strains in the loading direction between the small scale yielding and double-edge-notched specimen loaded into the region of general yielding.

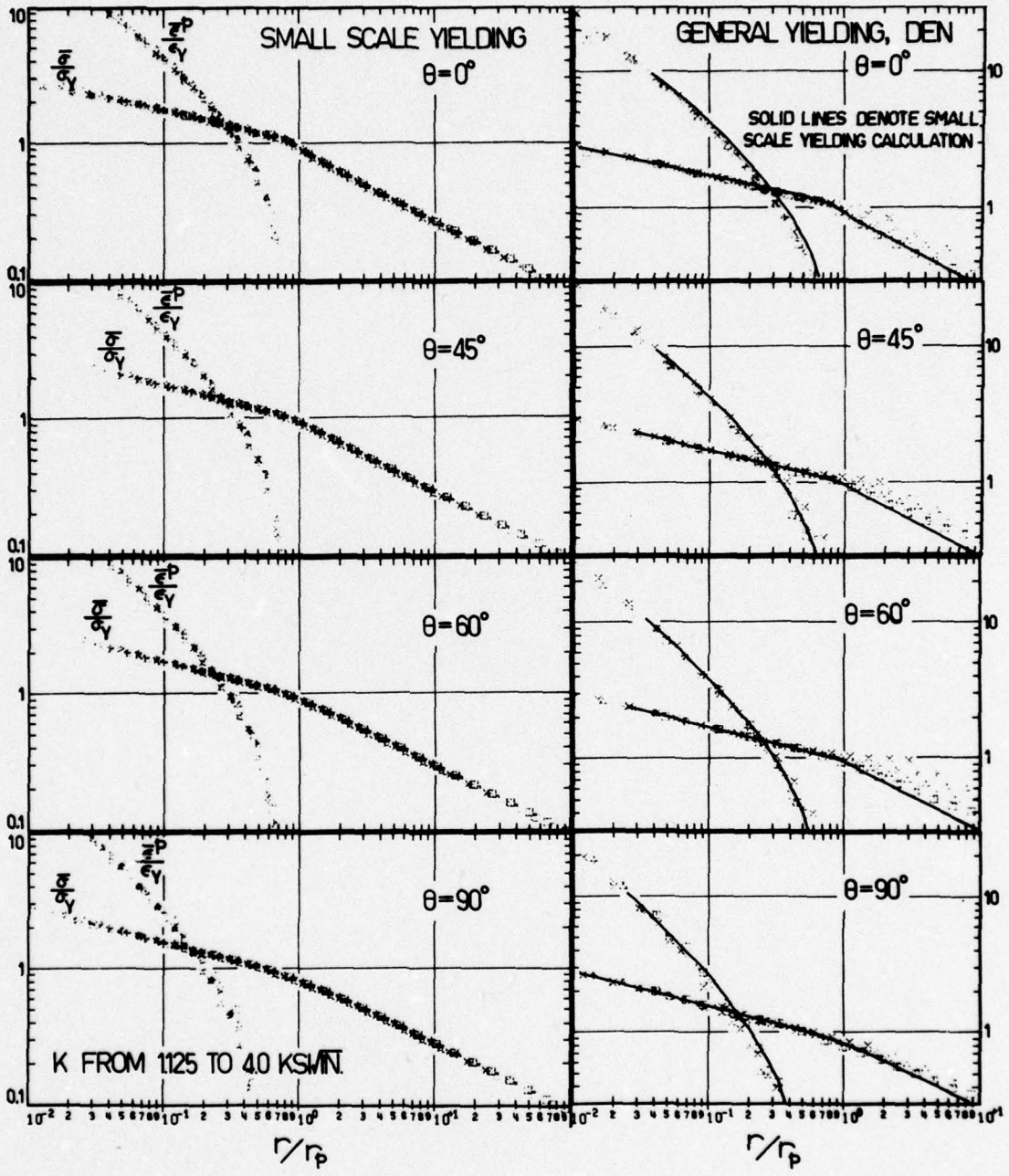


Fig. 5-6 Correlations of effective stress and effective plastic strain between the small scale yielding and double-edge-notched specimen loaded into the region of general yielding.

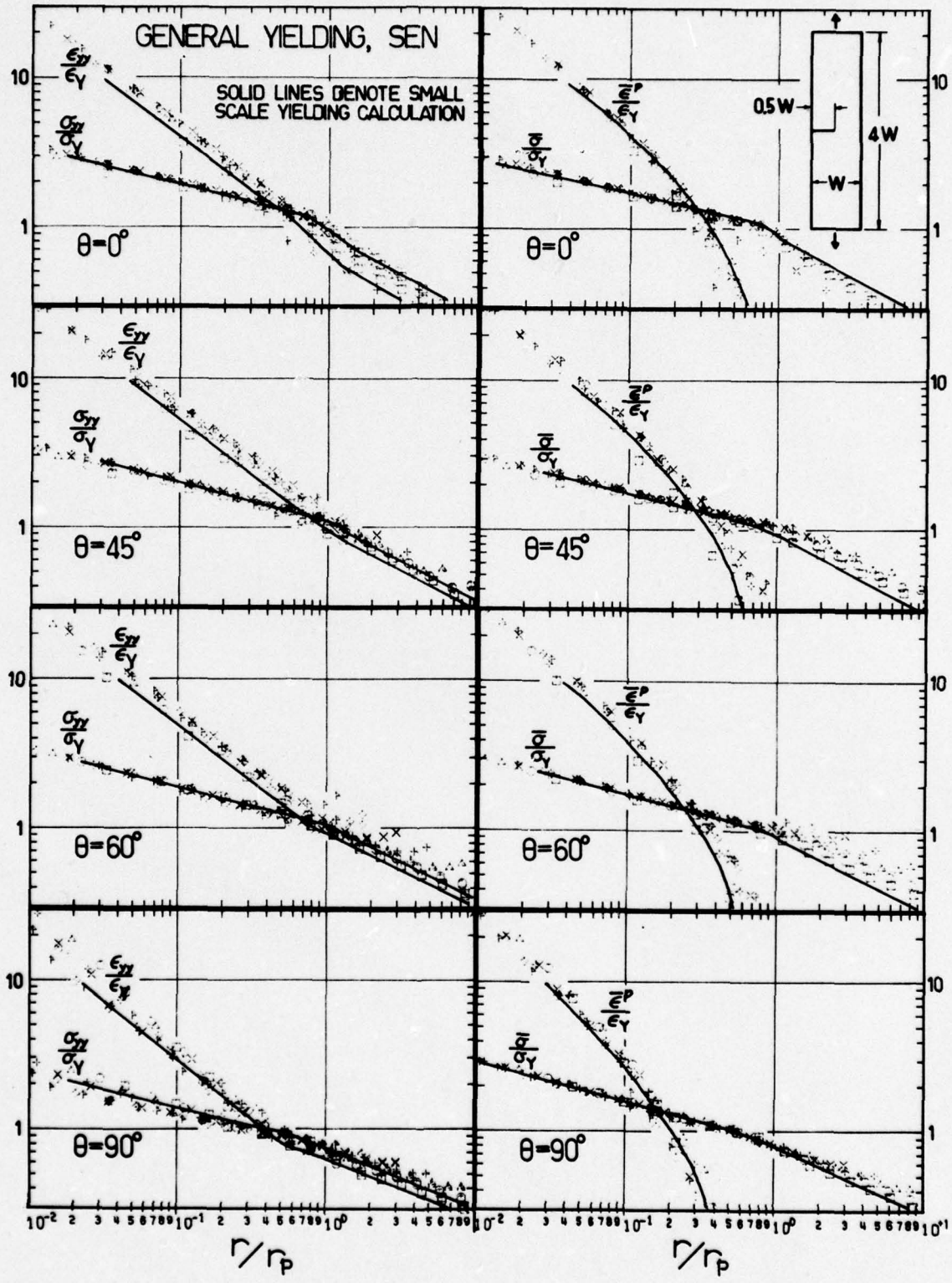


Fig. 5-7 Correlations of σ_{yy}, ε_{yy}, $\bar{\sigma}$ and $\bar{\varepsilon}^p$ between the small scale yielding and single-edge-notched specimen loaded into the region of general yielding.

Since the crack tip strain and stress distributions are the same in both specimens, it is fair to say that the K_I value of the small specimen in general yielding is the same as the K_I value of the large specimen. In this connection, Eq. 5-5 is applicable even in the case of general yielding as long as the corresponding pair of ε_{yy} and r, or σ_{yy} and r are taken from the characteristic plane stress region. By this approach, one is able to use a small sample to evaluate a very high fracture toughness. The equivalent K_I values for the empirical data in Fig. 4-6a are 38.5, 29.8 and 23.3 ksi$\sqrt{in}$, while the tensile yield stress of this material is 7.26 ksi.

Ke and Liu[5] used near tip strain as the correlation parameter between the plastically deformed region in small scale yielding and plane strain stiffened region in general yielding. Based on their limited empirical data, the characteristic strain distribution along the crack line in the plastically deformed region in small scale yielding is incorrectly taken as the extension of the inversed square root law of elastic behavior. The - 0.5 slope observed in the plastic region in their experiment is probably caused by the crack tip stiffening as well. Their approach yields a high estimate of equivalent stress intensity factor and fracture toughness.

5.3 NEAR TIP STRAIN AND STRESS AND THE FAR FIELD PARAMETERS

In Fig. 5-8 the normalized crack line strain, $\varepsilon_{yy}/\varepsilon_Y$, of DEN specimen calculated at various distances from the crack tip, r, is plotted against $\Delta/W\varepsilon_Y$ where Δ is the elongation of the DEN specimen over a gage length of seven inches and W is the specimen width. The results of the plane stress calculation which are represented by the solid lines agree well with the limited number of measurements, i.e. the triangular points in the figure. It is further demonstrated in this figure that in the region of general yielding beyond the arrow on the load-elongation curve in Fig. 4-7, the relation between ε_{yy} and Δ appears linear. A similar relation between the crack line stress, σ_{yy} at various distances, r, and th applied stress σ_∞ is shown in Fig. 5-9. These linear relationships suggest

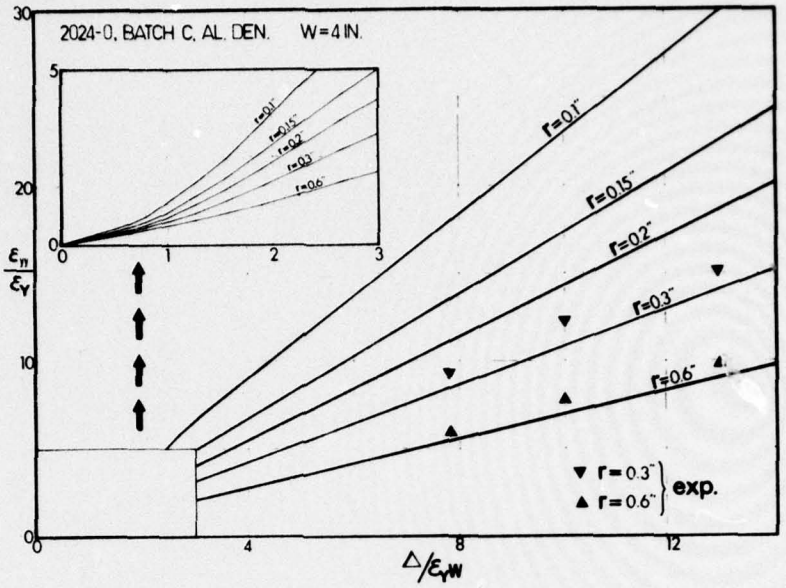


Fig. 5-8 The relation of near tip strain and gross elongation.

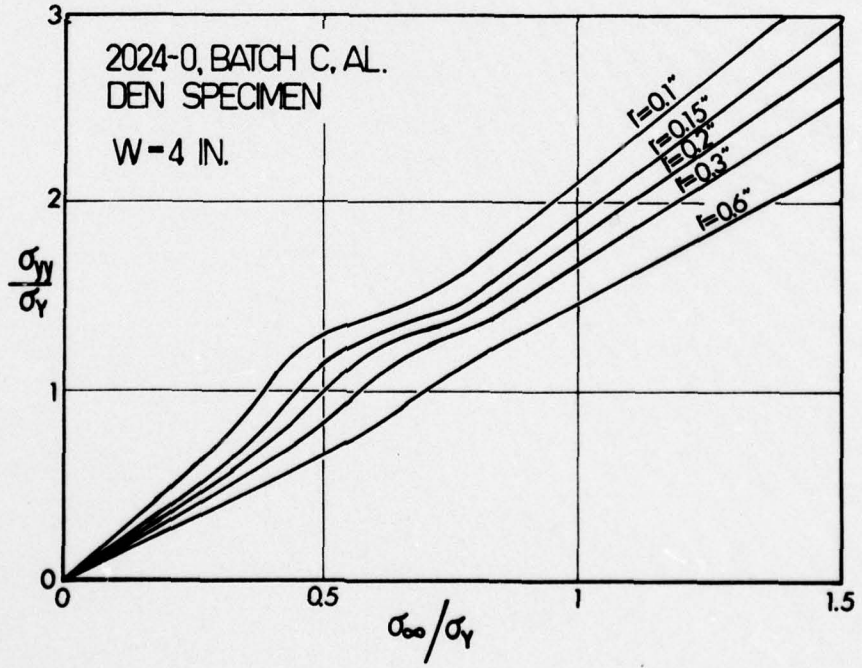


Fig. 5-9 The relation of near tip stress and applied stress.

that the assumption of proportional loading is justified for properly designed specimen loaded into the region of general yielding. In the linear regions, we have

$$\varepsilon_{yy} = \gamma \frac{\Delta}{W} \quad , \quad \text{and} \quad \sigma_{yy} = \gamma' \sigma_\infty \qquad 5\text{-}10$$

where γ and γ' are functions of r/W. Substituting Eqs. 5-10 into Eqs. 5-5, we have

$$K_\varepsilon = \varepsilon_{yy} r^m = \gamma r^m \frac{\Delta}{W} \qquad 5\text{-}11$$

For a given Δ, K_ε is constant, therefore $\Gamma \equiv \gamma r^m$ must be a constant. Combining Eqs. 5-5 and 5-11, we have

$$K_I^{2m}[(\varepsilon_Y \alpha^m/\beta)\sigma_Y^{-2m}] = \Gamma(\frac{\Delta}{W}) \quad . \qquad 5\text{-}12$$

In a like manner, the following relation can be derived

$$K_I^{2m'}[\sigma_Y \alpha^{m'}/\beta')\sigma_Y^{-2m'}] = \Gamma' \sigma_\infty \qquad 5\text{-}13$$

where $\Gamma' \equiv \gamma' r^{m'}$. For DEN specimen made of batch C aluminum, $\Gamma = 0.490$ and $\Gamma' = 1.315$; whereas for batch B aluminum the values of Γ and Γ' are 0.647 and 1.276 respectively. Multiplying Eqs. 5-12 and 5-13 and recall the relation $m + m' \simeq 1$, the final approximated form becomes

$$K_I^2/E = [\beta\beta'\Gamma\Gamma'/\alpha] \frac{\sigma_\infty \Delta}{W} \qquad 5\text{-}14$$

It is recognized that K_I^2/E is J in the case of plane stress. The quantity in the square bracket , $\beta\beta'\Gamma\Gamma'/\alpha$,is a constant for a given geometry and a given material. For the DEN specimen treated

$$K_I^2/E = 3.37 \frac{\sigma_\infty \Delta}{W} = 16.1 \left(\frac{\sigma_\infty}{\sigma_Y}\right)\left(\frac{\Delta}{W\varepsilon_Y}\right)$$

for batch C aluminum alloy and

$$K_I^2/E = 3.67 \frac{\sigma_\infty \Delta}{W} = 34.5 \left(\frac{\sigma_\infty}{\sigma_Y}\right)\left(\frac{\Delta}{W\epsilon_Y}\right)$$

for batch B aluminum alloy. Eq. 5-14 relates the equivalent stress intensity factor to the overall elongation and the applied stress for a small sample loaded far into the region of general yielding.

Fig. 5-10 plots the product of σ_{yy}/σ_Y and ϵ_{yy}/ϵ_Y as a function of the product of its associated far field parameters, σ_∞/σ_Y and $\Delta/W\epsilon_Y$. It is interesting to note that the deviation from linearity in Fig. 5-10 is not as severe as in the Figs. 5-8 and 5-9 where stresses and strains are plotted separately. The stresses and strains tend to compensate each other.

The stress intensity factor, K_I, are plotted at various loading levels in Fig. 5-11. The elastic solutions are also included in the plots for comparison. In the region of general yielding where the linear relationship between the near tip and far field parameters hold, the curves are approximated by the dashed lines represent Eqs. 5-14. When the linearity breaks down, the equivalent K_I values can still be obtained by the correlation of the characteristic near tip stresses and strains as given by Eqs. 5-5.

5.4 NEAR TIP STRAIN FRACTURE CRITERION

Ke and Liu[5] made near tip strains measurements at the onset of surface crack growth in three tough and ductile materials: HY-80 steel, and two batches of a fully annealed aluminum alloys (batch B and batch C). Fatigue pre-cracked specimens were tested under tensile load. Three types of specimens were tested: WOL, SEN and DEN. All the specimens of each material were of the same thickness. Their widths ranged from 2 to 8 inches.

At the first sign of surface crack growth, the near tip strains were measured with the moire method. The results are shown in Fig. 5-12. The cross

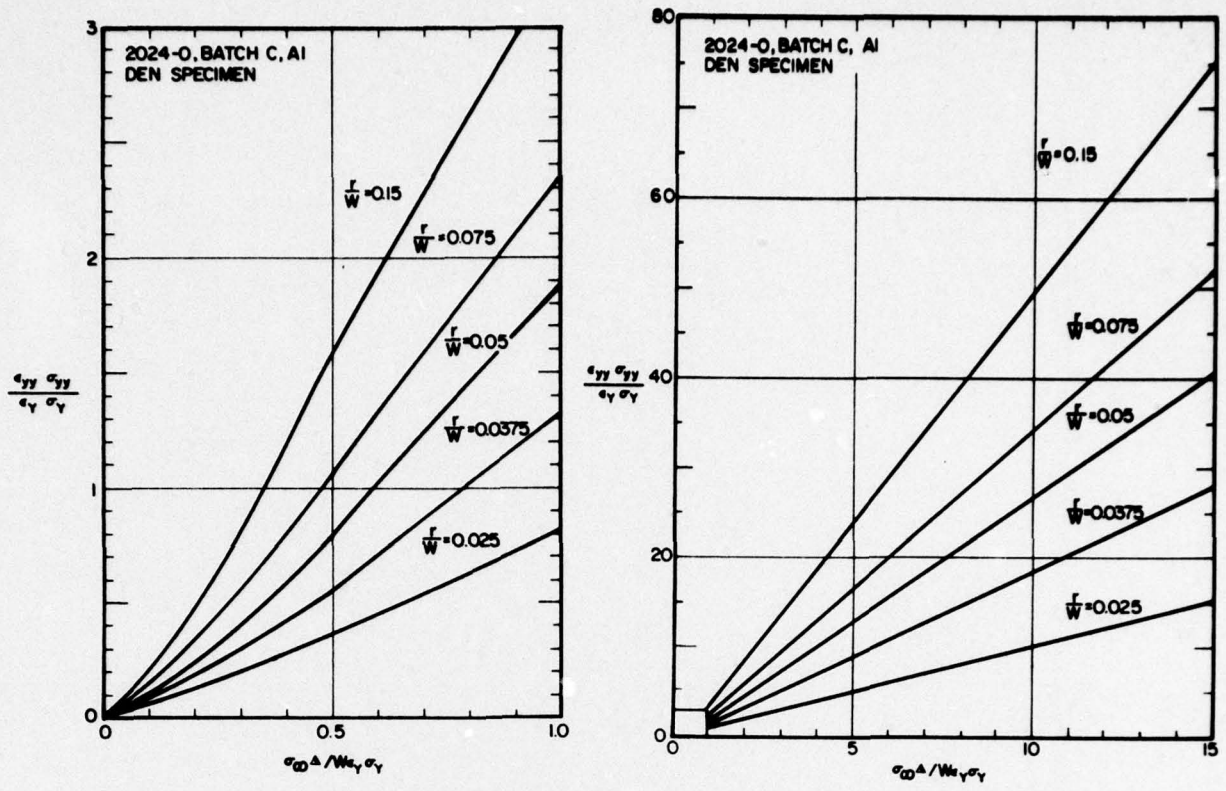


Fig. 5-10 Near field parameter, $\sigma_{yy}\varepsilon_{yy}/\sigma_Y\varepsilon_Y$ versus far field parameter, $\sigma_\infty\Delta/W\sigma_Y\varepsilon_Y$.

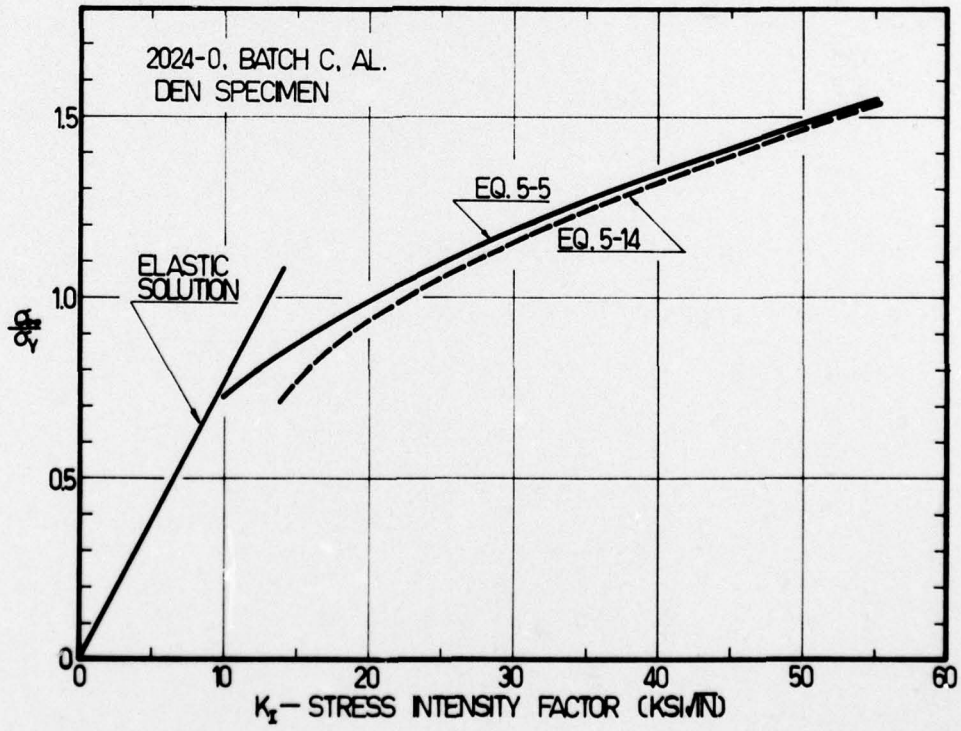


Fig. 5-11 Calculated stress intensity factor at various loading levels.

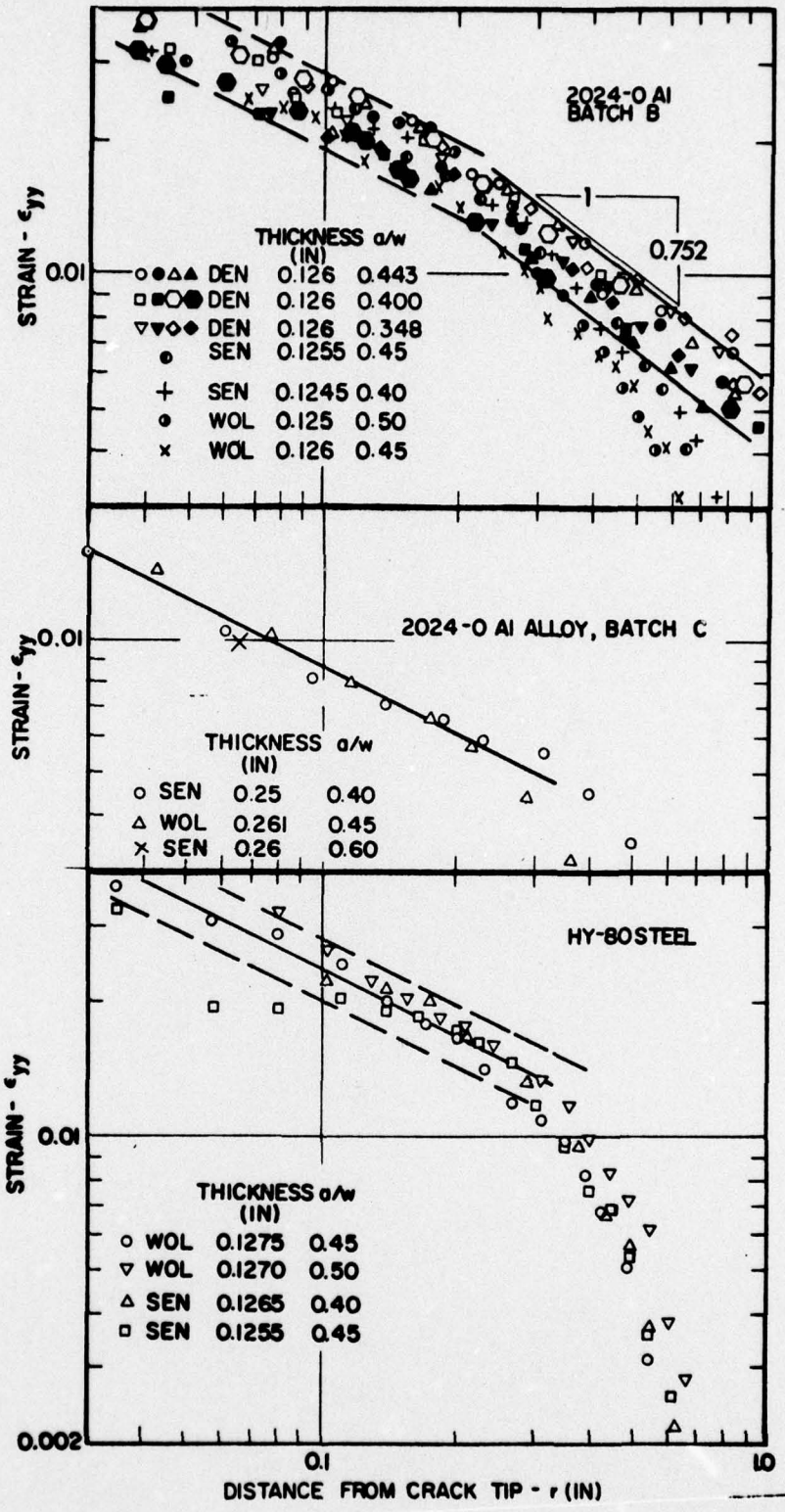


Fig. 5-12 Near tip strain measurements at the onset of slow crack growth on specimen surface.

in the second figure for batch C 2024-0 aluminum alloy was measured with a small strain gage, which agrees well with the moire strain measurements.

The strain measurements for each of these three materials fall within a narrow band in spite of the differences in specimen geometry and size. This indicates that at the first appearance of crack growth on the specimen surface, near tip strain is not affected by specimen geometry and the type of loading as long as the specimens are of the same thickness.

A careful study of the data presented in Fig. 5-12 reveals that the three dimensional stiffening effects are shown in all the three types of specimen at the immediate vicinity of the crack tip. For the WOL and SEN specimens, the bending effect is so dominate that there is no plane stress deformed region can be detected as it is reflected from the strain measurements. A longer ligament width should be considered for this observation. For the DEN type specimen, the characteristic plane stress deformed region is noticable at approximately one thickness away from the crack tip. The K_c value of this particular material (Batch B aluminum alloy) is estimated to be 69.1 ksi$\sqrt{in}$ according to Eq. 5-5. The value of $(\frac{K_c}{\sigma_Y})^2$ is close to 50 inches. According to the requirement of the linear elastic fracture mechanics, a ligament size of 10 feet is necessary to conduct a valid fracture toughness measurement.

5.5 REFERENCES

1. Hutchinson, J. W., "Singular Behavior at the End of a Tensile Crack in a Hardening Material," J. of Mech. and Phys. of Solids, vol. 16, p. 13, (1968).

2. Rice, J. R. and Rosengren, G. F., "Plane Strain Deformation Near a Crack Tip in a Power-Law Hardening Material," J. of Mech. and Phys. of Solids, vol. 16, p.1 (1968).

3. Tracey, D. M., "Finite Elements for Determination of Crack Tip Elastic Stress Intensity Factors," Eng. Fract. Mech., vol. 3, p. 255. (1971).

4. Larsson, S. G. and Carlsson, A. J., "Influence of Non-Singular Stress Terms and Specimen Geometry on Small-Scale Yielding at Crack Tip in Elasto-plastic Materials," J. of Mech. and Phys. of Solids, vol. 21, p. 263 (1973).

5. Ke, J. S. and Liu, H. W., "Near Tip Strain as a Ductile Fracture Criterion," Int. J. of Fracture, vol. 7, p. 487 (1971).

CHAPTER VI CRACK OPENING DISPLACEMENTS AND J-INTEGRALS

6.1 CRACK OPENING DISPLACEMENTS

Crack opening displacements (COD) were studied for both batches of aluminum alloys (batch B and C). The calculated crack tip profiles at various loading levels were compared with the earlier measurements by Gavigan[1] in Fig. 6-1. A close agreement was noticed.

Figs. 6-2 and 6-3 show the correlations of COD between the small scale yielding and double-edge-notched specimen in general yielding for batch C aluminum alloy. The distinct deformation characteristics in the elastic and plastic portions of the specimen are clearly shown. In the plastically deformed region, one has

$$\frac{COD}{COD^*} = \left(\frac{r}{r_p}\right)^{-m''} \qquad 6\text{-}1$$

where -m" is the slope in Figs. 6-2 and 6-3 in the near tip region and

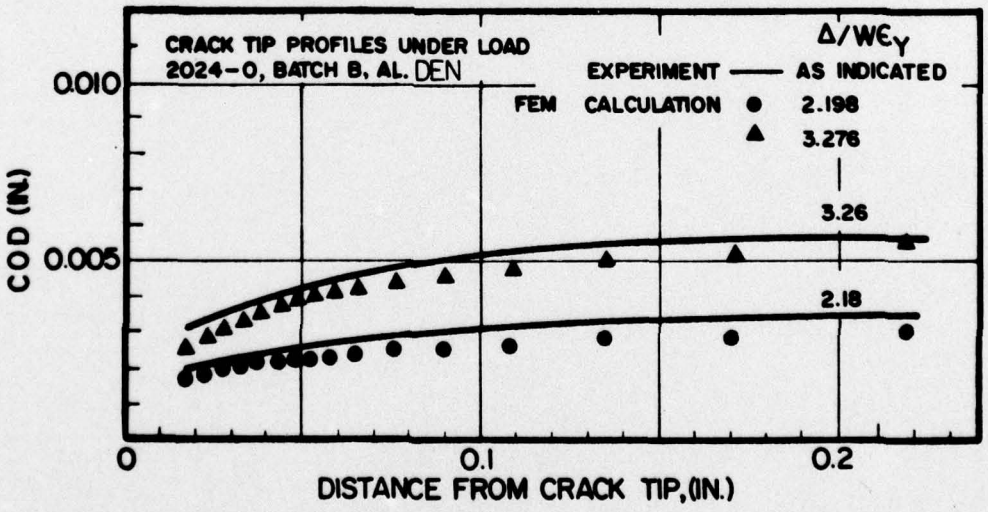


Fig. 6-1 Measured and calculated crack tip profiles, batch B aluminum alloy.

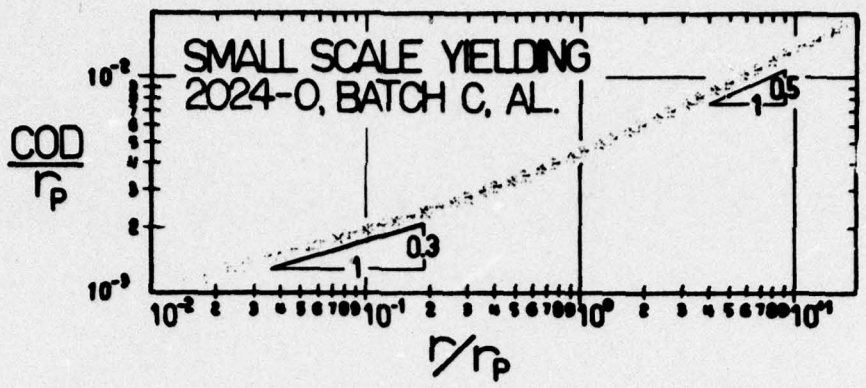


Fig. 6-2 COD as a function of r, both normalized by r_p, from the small scale yielding calculation.

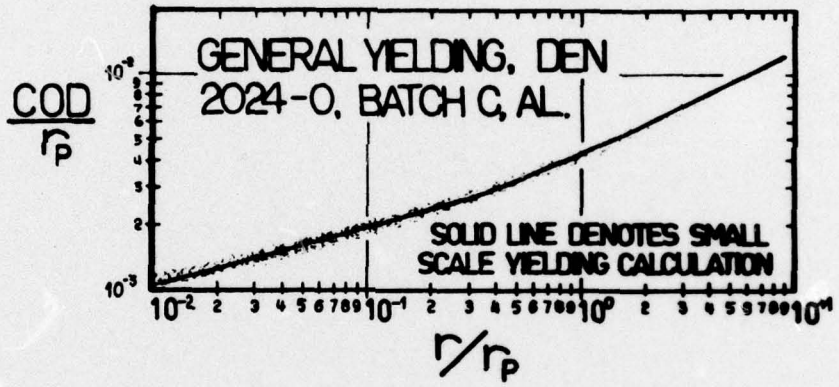


Fig. 6-3 The correlations of COD between the small scale yielding and double-edge-notched specimen in general yielding.

COD* is the crack opening displacement at $r = r_p$. Define

$$Q \equiv \frac{COD^*}{r_p} \quad . \qquad 6\text{-}2$$

Substitute Eqs. 5-3, 6-2 into Eq. 6-1 and rearrange

$$K_I = \sigma_Y \alpha^{-1/2} Q^{1/2m''-2} r^{m''/2m''-2} \, COD^{1/2-2m''} \qquad 6\text{-}3$$

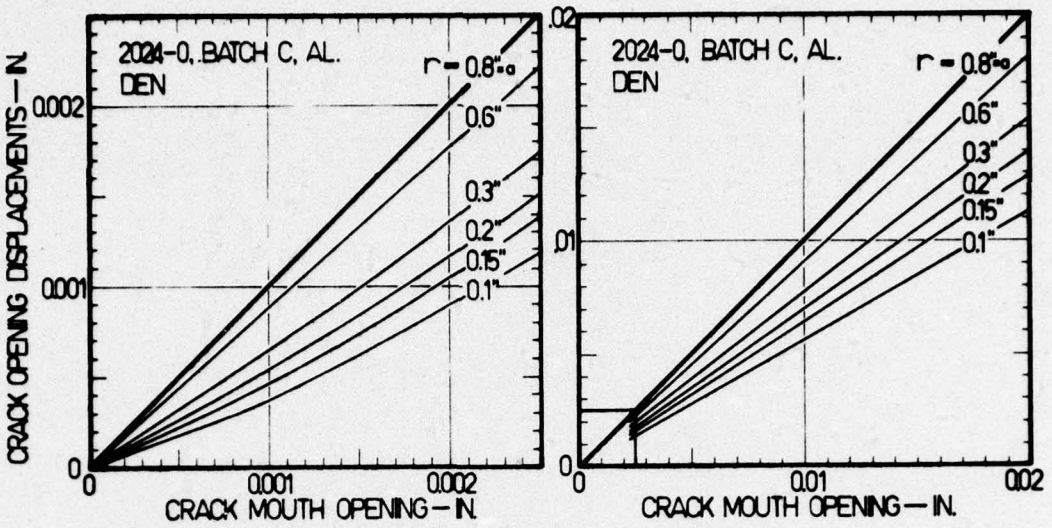


Fig. 6-4 Cacculated COD as a function of Crack Mouth Opening at various distances from the crack tip.

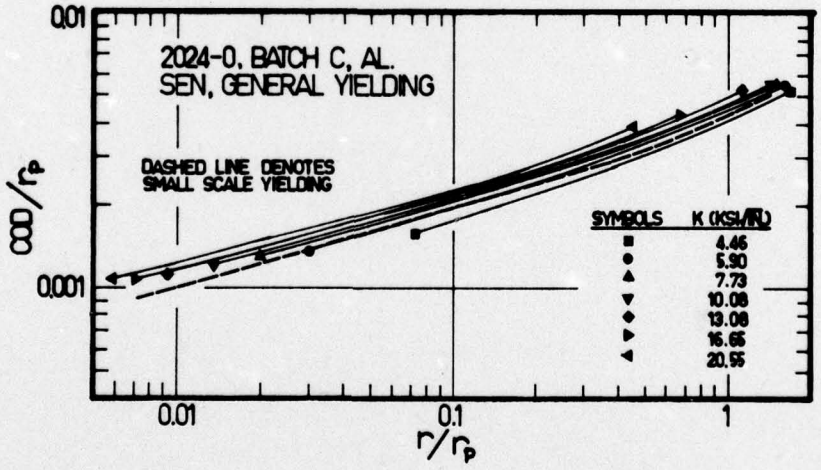


Fig. 6-5 The correlations of COD between the small scale yielding and single-edge-notched specimen in general yielding.

where α was defined in the previous chapter. For batch C aluminum $m'' = 0.298$ and $Q = 0.0036$. Therefore, in addition to crack tip opening displacements (CTOD), proposed by Wells,[2] COD in the near tip region can be used to evaluate fracture toughness as well.

6.2 COD AND CRACK MOUTH OPENING

Consider the extreme case while r is equal to the notch depth or crack length, a. In this particular situation, COD is replaced by its corresponding far field parameter, crack mouth opening (CMO). Eq. 6-3 now becomes

$$K_I = \sigma_Y \sqrt{a/\alpha} \left[\frac{CMO}{Qa}\right]^{1/2-2m''} \qquad 6\text{-}4$$

It should be pointed out that although COD and CMO are identical when r = a in spite of small scale yielding or general yielding, Eq. 6-4 is valid provided that the condition of Eq. 6-1 is satisfied. In other words, the application of Eq. 6-4 is restricted to the range of general yielding.

Fig. 6-4 plots the calculated COD as a function of CMO at various distances from the crack tip. The linearity breaks down for small r in low loading levels.

The correlation of COD between SEN specimen in general yielding and small scale yielding is shown in Fig. 6-5. The equivalent K values in the figure are calculated from near tip correlation approach following Eqs. 5-5. It appears in Fig. 6-4 that the deviation from the small scale yielding results increases with K. The match is not as good as it is in the case of DEN specimen. It is believed that the excessive amount of COD being attributed to the rotation due to the bending. Some cognition of stress and strain field ahead of crack tip are required in order to estimate the amount of rotation.

6.3 COD AND NEAR TIP STRAIN

In the immediate vicinity of the crack tip where the three-dimensional effects prevail, specimen thickness plays an important rule in the deformation profile. This is illustrated in Figs. 6-6 and 6-7 where COD and strain in

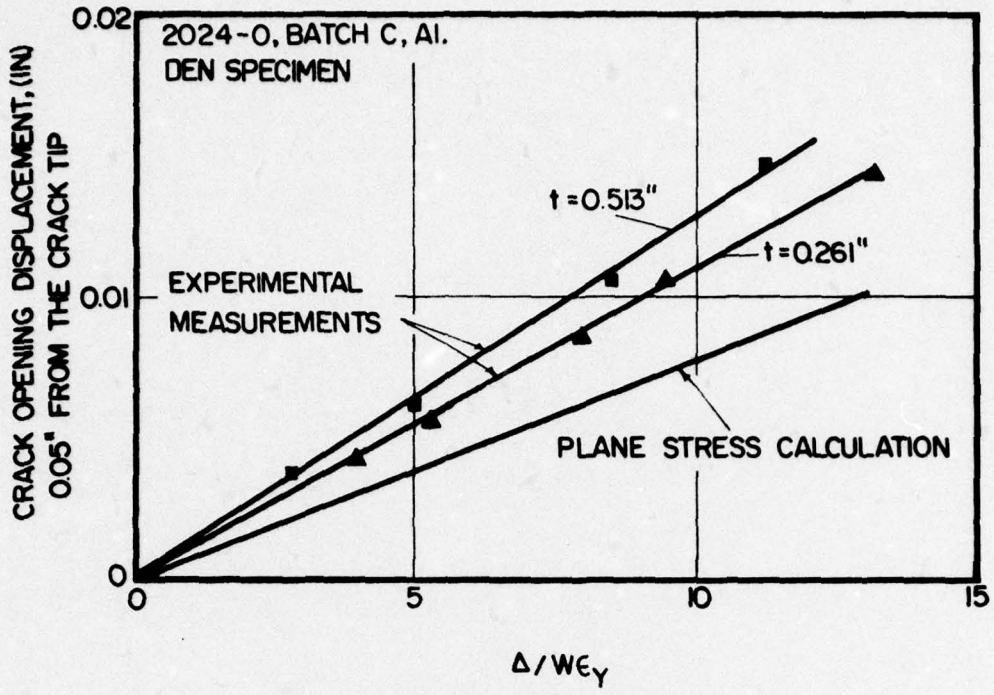


Fig. 6-6 The effect of crack tip stiffening on COD in general yielding.

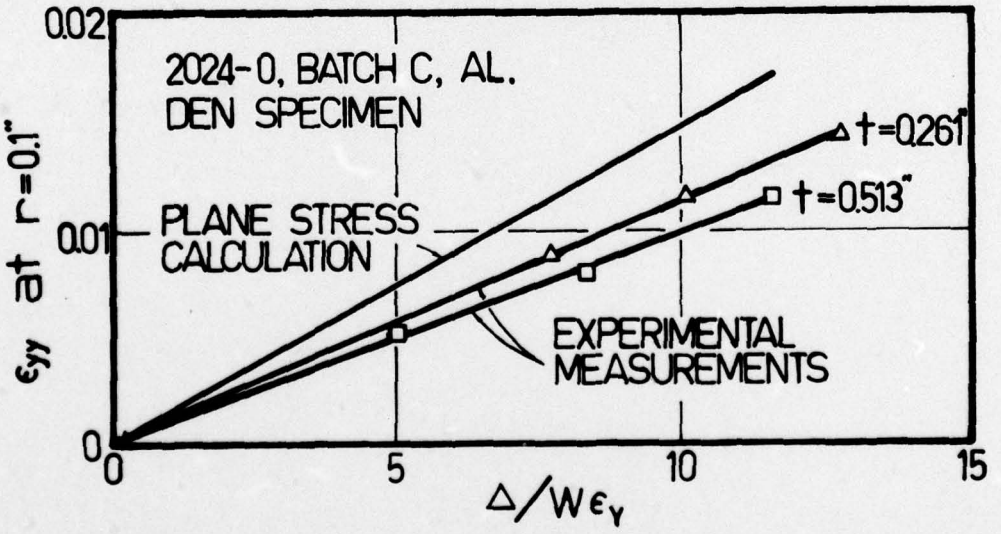


Fig. 6-7 The effect of crack tip stiffening on near tip strain in general yielding.

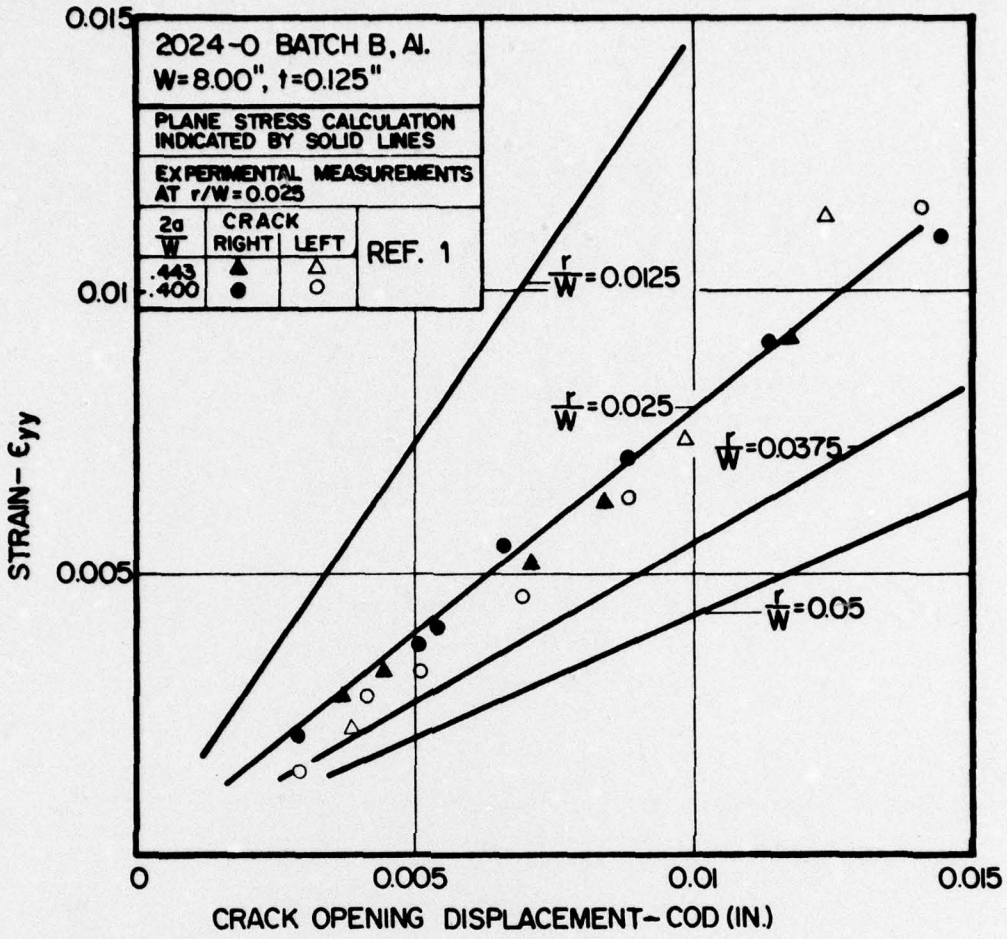


Fig. 6-8 ε_{yy} versus COD at various r.

loading direction are plotted at various loading levels for a DEN specimen loaded into the region of general yielding. As the thickness increases, the strain decreases; whereas COD increases at a given loading level.

A linear relation was found between the COD and the strain in loading direction by both empirical measurements and FEM calculations. Fig. 6-8 shows the measured and calculated near tip strain, ε_{yy}, and near tip COD both at different values of r. The empirical data shown are outside the crack tip stiffening zone. This linear relationship could be derived as well from Eqs. 1-3. Eqs. 1-3 also suggests that the product of the slopes of each line in

Fig. 6-8 and its corresponding value of r should yield a constant. It is indeed so and equal to 0.02 from the calculated results.

6.4 J-INTEGRAL

Rice's[3] contour integral J are evaluated from the field values obtained by the finite element analysis. Rectangular path is chose for the programming convenience. The detail procedures of calculation were reported by Hayes.[4] The number of paths evaluated at each loading level are 18 for small scale yielding and 10 for general yielding. The paths are shown in Fig. 6-9. Path dependency are less than 3% in all the cases studied.

In the case of small scale yielding and under the plane stress conditions, the stress intensity factor K is related to J by

$$J = \frac{K^2}{E} \qquad 6\text{-}5$$

From the previous discussion, the equivalent stress intensity factor can be evaluated from the stress or strain field ahead of a crack tip as well as COD behind the tip. Therefore, Eq. 6-5 is used to obtain the equivalent J values in the region of general yielding.

The results are plotted in Fig. 6-10. Solid line indicates the values of J calculated from contour integral. The curves represent the K^2/E obtained from near tip stress or strain (Eq. 5-5) and from far field parameters (Eq. 5-14) are denoted by dashed line and dash-dotted line respectively. Results from COD calculation following Eq. 6-3 is plotted in dotted line. The disticntion between the curves from near tip stress and strain cannot be recognized in this scale of plot. In general, they agree reasonably well with the value obtained from contour integral; whereas, the curve calculated from COD tends to deviate from the curve obtained from contour integral at high loading level. As it is pointed out in the foregoing chapter, the results from far field parameter are higher than the others in the low loading range. Overall speaking, the difference between the various calculations are within 20%.

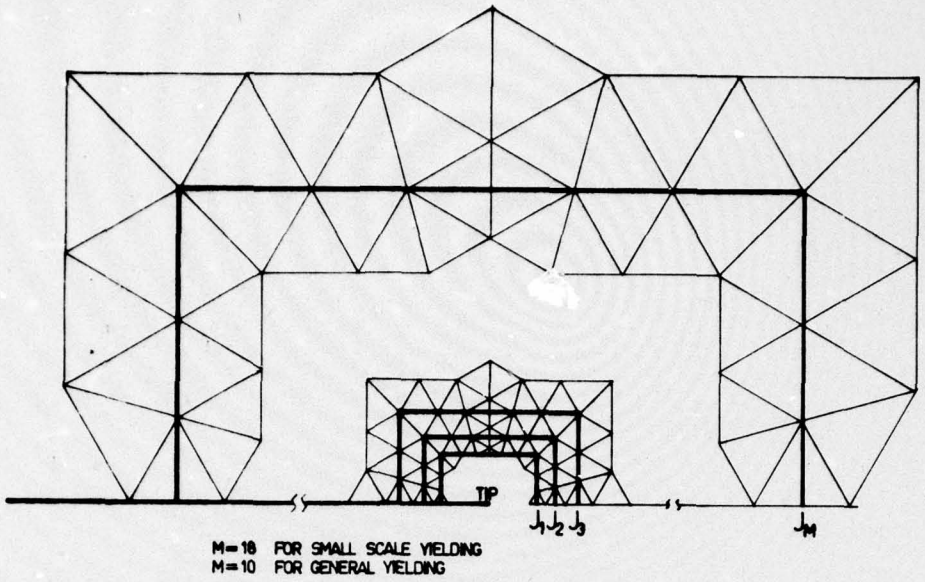


Fig. 6-9 Integral paths of J.

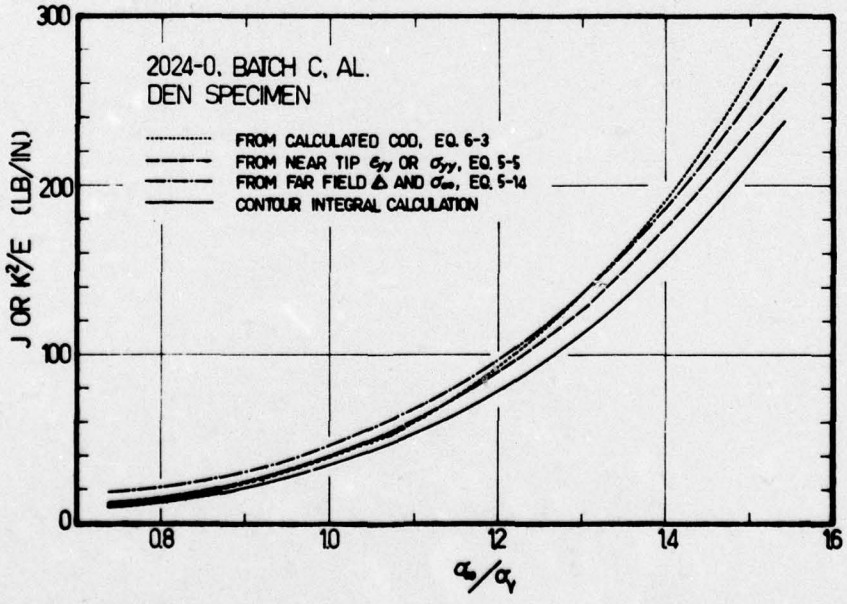


Fig. 6-10 Calculated J -- a comparison of different approaches.

6.5 REFERENCES

1. Gavigan, W. J., "Crack Tip Deformation in Metallic Plates Beyond General Yielding with Applications to Ductile Fracture," Ph.D. Dissertation, Syracuse University (1970).

2. Wells, A. A., "Application of Fracture Mechanics at and Beyond General Yielding," British Welding J., p. 563, Nov. (1963).

3. Rice, J. R., "A Path Independent Integral and the Approximate Analysis of Strain Concentration by Notches and Cracks," Journal of Applied Mechanics, Transaction of ASME, pp. 379-386, June (1968).

4. Hayes, D. J., "Some Applications of Elastic-Plastic Analysis of Fracture Mechanics," Ph.D. Dissertation, Imperial College, University of London, (1970).

CHAPTER VII CONCLUDING REMARKS

1. The immediate vicinity of crack tip region is stiffened against plastic deformation. The region affected by the crack tip stiffening extends from the crack tip to a distance approximately equal to the thickness of the specimen. A qualitative study on the effect of triaxial state of stress in the region has been made. The influence of the specimen thickness on the crack tip stiffening effect has been explored.

2. The crack tip stiffened zone is imbedded in the characteristic plane stress zone if the ratio of the total net cross-sectional width and the specimen thickness is larger than ten. This size requirement provides a guideline for laboratory specimen design.

3. For the specimens of the same thickness with the same stress and strain fields in the characteristic plane stress zone, the stresses and strains in the stiffened zones of all the specimens must be the same.

4. A link between linear elastic fracture mechanics and ductile fracture criterion can be established by the stress and strain distributions near a crack tip in the characteristic plane stress region. In this region, the stress or strain at the same value of r/r_p is the same regardless of the size of r_p. This is true both in the case of small scale yielding and general yielding. With this knowledge, the equivalent K_I value or fracture toughness of a small testpiece loaded considerably into general yielding can be obtained by the correlation of stress or strain in the characteristic plane stress region.

5. A linear relationship has been found respectively between the near tip stress and strain and the applied load and the overall elongation of a specimen loaded far into the general yielding. The sufficient conditions for the validity of this relationship have been discussed. As a consequence, the equivalent stress intensity factor can be related directly to the boundary load or elongation.

6. Crack tip stress and strain for a specimen loaded into the region of general yielding can be characterized by J-integral, COD, or any of the near tip stresses or strains. Therefore, any one of these physical parameters can be used as a ductile fracture criterion if the crack tip stress or strain environment concept is employed. The inter-relations between these quantities are examined.